Am J Cancer Res 2023;13(4):1387-1406
www.ajcr.us /ISSN:2156-6976/ajcr0148058

Original Article

Metabolic genes, a potential predictor of prognosis and immunogenicity of clear cell renal cell carcinoma

Cheng-Jian Ji[1*], Xi-Yi Wei[1*], Liang-Yu Yao[1*], Yi-Chun Wang[1], Rong Cong[1], Ning-Hong Song[1,2]

[1]Department of Urology, The First Affiliated Hospital of Nanjing Medical University, Nanjing 210029, Jiangsu, China; [2]The Affiliated Kezhou People's Hospital of Nanjing Medical University, Kezhou 845350, Xinjiang, China. [*]Equal contributors.

Received November 27, 2022; Accepted April 2, 2023; Epub April 15, 2023; Published April 30, 2023

Abstract: Clear cell renal cell carcinoma (ccRCC) is the most common subtype of renal cell carcinoma (RCC). Many ccRCCs are diagnosed at an advanced stage due to the lack of early symptoms, with a high mortality rate and a poor prognosis. The occurrence and development of ccRCC are closely related to metabolic disorders. This study aims to explore the relationship between metabolic genes and prognosis, immune microenvironment, and tumor development of ccRCC. Using data from TCGA, GEO, and ArrayExpress, we successfully established a risk model (*riskScore*) based on 4 metabolic genes (MGs) that can accurately predict the prognosis and immune microenvironment of ccRCCs. In addition, we determined the role of PAFAH2 in suppressing tumor cell proliferation and migration in ccRCC in vitro. Our research may shed new light on ccRCC patients' prognosis and treatment management.

Keywords: Metabolic genes, ccRCC, prognosis, TME, PAFAH2

Introduction

Renal cell carcinoma (RCC) is a common tumor in the urinary system, ranking among the top ten cancer diagnoses in the world [1]. Clear cell renal cell carcinoma (ccRCC) is the most common histological subtype in RCC, accounting for about 80%. Survival outcomes of ccRCC are poor compared to other subtypes of RCC, including papillary renal cell carcinoma, chromophobe renal cell carcinoma, and collecting duct carcinoma [2]. Due to the lack of obvious clinical symptoms, many patients are already in advanced stages at the time of diagnosis [3, 4]. Targeted therapy has been the standard first-line treatment for advanced ccRCC for nearly a decade. However, almost all patients eventually develop drug resistance [5]. With the rise of immune checkpoint inhibitors therapy, renal cancer has entered a new era of immune-targeted therapy. Recent studies have shown that PD-1 inhibitors can alleviate the progression in some patients with advanced renal cancer [6, 7]. Unfortunately, there are still many patients who do not respond well to immunotherapy. Differences in the tumor microenvironment have been suggested as a possible reason for the heterogeneity of ccRCC responses to immunotherapy [8].

Glycolysis, fatty acid metabolism, tyrosine metabolism, nucleotide anabolism, and other metabolic pathways are necessary to maintain normal cell homeostasis [9, 10]. Many scientists believe that abnormal metabolic processes could be a key factor in the development of cancer [11-13]. A typical feature of ccRCC is the presence of significant lipid, glycogen, and other metabolic pathways disorders. In breast cancer and colorectal cancer, abnormal metabolic pathways have been reported to be associated with poor prognosis [14, 15]. Due to the significant abnormal expression of metabolites in tumor tissues at different stages, Marin-Rubio et al. suggested that metabolic genes (MGs) could be used as prognostic markers for cancer [16]. The prognostic value of MGs has been verified in a variety of cancers, including prostate cancer, lung adenocarcinoma, liver cancer, head and neck squamous cell carcinoma, and rectal cancer [17-21].

Von Hippel-Lindau (VHL), which encodes the E3 ubiquitin ligase that recognizes hypoxia-induc-

ible factor (HIF) proteins, is one of the genes closely related to the occurrence of ccRCC [22]. About 90% of cases have mutations in VHL [23]. Loss of VHL gene function will cause the accumulation and activation of HIF proteins in cancer cells, mistakenly sending hypoxia signals that activate angiogenesis and stimulate tumor growth [24, 25]. In addition, there are a lot of lipids and glycogen in the cytoplasm of ccRCC. The hypoxic response induced by the mutation of VHL and the pathology of ccRCC indicate that there is a disorder of the metabolic environment in ccRCC. ccRCC has been demonstrated that it is usually accompanied by reprogramming of glucose metabolism, reprogramming of fatty acid metabolism, and reprogramming of the tricarboxylic acid cycle. The metabolism of tryptophan, arginine and glutamine is also reprogrammed in many ccRCCs [26, 27]. Therefore, alterations in these metabolic pathways provide new possibilities for ccRCC treatment strategies and biomarkers. In addition, metabolic disturbances in ccRCC may be associated with increased immune evasion of tumor cells [28]. Which suggests that dysregulated MGs in ccRCC may be used to predict response to immune checkpoint inhibitors therapy.

Our study aims to explore the relationship between MGs and prognosis, TME, and tumor development of ccRCC.

Materials and methods

Acquisition and preparation of data

Transcriptome profiling data and related clinical information of ccRCCs were downloaded from The Cancer Genome Atlas (TCGA) Data Portal (https://tcga-data.nci.nih.gov/tcga/; accessed January 2020), GEO database (https://www.ncbi.nlm.nih.gov./geo/; GSE29609) and ArrayExpress database (https://www.ebi.ac.uk/arrayexpress/; E-MTAB-1980). A total of 944 genes related to metabolism were obtained from the KEGG gene sets of GSEA database (https://www.gsea-msigdb.org/gsea/downloads.jsp; accessed January 2020). In addition, R software used to process transcriptome data. The "sva" package was used to correct the transcriptome data from different databases. The "Limma" package was used for further difference analysis.

Identification of MGs with prognostic value

Patients with less than 90 days of follow-up were first excluded. Then, the univariate cox regression analysis was used to identify prognostic genes from differentially expressed MGs. "Survival" package in R software was used for univariate cox regression analysis.

Protein-protein interaction (PPI) and cluster analysis of hub genes

STRING database (http://www.stringdb.org/) was used to construct a PPI network of prognostic MGs. CytoHubba in Cytoscape software was used to explore hub genes in the PPI network. In addition, MCODE was used to generate clusters of hub genes.

Establishment of an independent prognostic index (PI, riskScore) based on MGs in training cohort

Patients in TCGA cohort with complete clinical information such as age, gender, pathology stage, histological grade, and TMN stage were randomly divided into training cohort and testing cohort by R software. The basic requirements of grouping include two aspects. First, we control the ratio of the number of people in training cohort to the number of people in testing cohort to about 7:3. Then, from the perspective of the distribution of patients in various clinical features, the patient composition in the training cohort and the patient composition in the testing cohort should be similar.

To further identify the key prognostic MGs, the lasso regression and the multivariate cox regression analysis were performed. The prognostic model was established using the weight coefficients of each gene in the multivariate cox regression analysis. The PI was calculated using the following formula: $\beta_1 \times gene_1$ expression + $\beta_2 \times gene_2$ expression + ····· + $\beta_n \times gene_n$ expression, where β corresponded to the weight coefficient.

Validation of key genes at the protein level

The Human Protein Atlas (HPA) database (https://www.proteinatlas.org/) was used to verify the protein level of key MGs in the established prognosis index.

Evaluation of the prognostic index in the training cohort

According to our prognostic model, each patient would get a risk score. The median risk score was set as the cutoff value for dividing ccRCC patients into a high-risk group and a low-risk group. Kaplan-Meier (K-M) method was utilized to plot the survival curves. The log-rank test was performed to assess differences in the survival rates between the high-risk group and the low-risk group. The time-dependent receiver operating characteristic curves (ROC) were created by the "survivalROC" package. The area under the curve (AUC) values were calculated to evaluate the specificity and sensitivity of the model. Decision Curve Analysis (DCA) was performed by the "ggDCA" package. The risk score distribution of patients, Survival status scatter plots for patients in the prognostic model and the heatmap of prognosis-related MGs were also displayed.

Verification of the prognostic ability of this model in the testing cohort and the entire cohort

To verify the performance of *riskScore* in the testing cohort, survival curves were plotted using the "survival" package and "survminer" package. A time-dependent ROC curve was also performed. We then repeated the verification work in the entire cohort (including TCGA cohort and GEO cohort).

In addition, the correlation between the prognostic model (risk genes and *riskScore*) and each clinical feature was analyzed.

To further evaluate whether our model could be used as an independent prognostic factor, we included age, gender, pathology stage, histological grade, T, M, N, and *riskScore* as independent variables. Univariate cox regression analysis and multivariate cox regression analysis were then performed on changes in overall survival time and overall survival outcomes.

Verification of the prognostic ability of this model in the ArrayExpress cohort

According to our prognostic model, each patient in ArrayExpress cohort will get a risk score. Then, we use the cutoff value from training cohort to divide ccRCC patients into a high-risk group and a low-risk group. K-M method was utilized to plot the survival curves. And the log-rank test was performed to assess differences in the survival rates between high-risk group and low-risk group. The time-dependent ROCs were created by the "survivalROC" package. The AUC values were calculated to evaluate the specificity and sensitivity of the model. Next, K-M survival curve analysis was used to assess the prognostic value of each risk gene.

Nomogram development and validation for prognostic risk prediction

By "rms" package, a prognostic nomogram was also performed to visualize the relationship between individual predictors and overall survival rates in ccRCC patients based on the cox proportional hazard regression model.

GO and GSEA enrichment analysis

The R packages "org.Hs.eg.db" and "clusterProfiler" were used for GO annotation and GO enrichment analysis of differential genes. Gene-set enrichment analysis (GSEA) was used to explore the mechanisms that lead to different outcomes between patients in the high-risk group and patients in the low-risk group.

Somatic variants analysis

To explore the differences in gene mutation frequencies between patients in different groups, the somatic variants data of ccRCC patients in TCGA database were downloaded. The R package "maftools" was used to analyze mutation data.

Tumor immune analysis

Immune cell infiltration in ccRCC was explored by CIBERSORT, a method that has been widely used to evaluate immune cell infiltration in complex tissues [29]. Tumor Immune Dysfunction and Exclusion (TIDE) is a module that predicts patient response to immunotherapy based on transcriptome data [30]. TIDE scores of ccRCC patients was obtained from an online application (http://tide.dfci.harvard.edu/).

Drug sensitivity prediction

We predicted the response of ccRCC patients to targeted drugs using the Genomics of Drug Sensitivity in Cancer (GDSC) database

(https://www.cancerrxgene.org). R package "pRRophetic" was used to estimate the half-maximal inhibitory concentration (IC50).

Cell culture and siRNA transfection

Two ccRCC cell lines (786-O and 769-P) were purchased from the National Collection of Authenticated Cell Cultures (Shanghai, China). RPMI-1640 (Gibco, USA) medium containing 10% FBS (Gibco, USA) was used for cell culture. All cells were cultured in a constant temperature incubator (Thermo, USA) at 37°C with 5% carbon dioxide concentration.

SiRNAs used to interfere with intracellular PAFAH2 expression levels were synthesized by genepharma (Shanghai, China). The sequences corresponding to the siRNAs used in this study were as follows: si-PAFAH2-1, 5'-GAAAGAAGACUAUAAUCAAUG-3'; si-PAFAH2-2, 5'-CGAGGACCUGUGUUCUUUAUC-3'. Lipofectamine 3000 (Invitrogen, USA) and serum-free opti-MEM (Gibco, USA) medium were used to prepare transfection complexes.

RNA extraction, reverse transcription, and real-time quantitative PCR detecting system (RT-qPCR) assays

Total RNA from cells and tissues was extracted by using TRIzol reagent (Invitrogen, America). Total RNA was reverse transcribed into cDNA using a special reverse transcription kit (Vazyme Biotech, China). RT-qPCR was performed according to the protocol of ChamQ SYBR qPCR Master Mix (Vazyme Biotech, China). In this study, β-actin was used as an endogenous control. The $2^{(-\Delta\Delta CT)}$ method was used to analyze the relative expression levels of genes. The sequences of primers were as follows: PAFAH2, Forward primer 5'-GGGGCTGCTTCTGAGGAATC-3', Reverse primer 5'-GTCGAAAGAAGCTCCCCTGG-3'; β-actin, Forward primer 5'-CTCCATCCTGGCCTCGCTGT-3', Reverse primer 5'-GCTGTCACCTTCACCGTTCC-3'.

Western blot and immunohistochemistry assays

Total proteins from cells and tissues were extracted using RIPA lysis buffer containing 1% Phenylmethanesulfonylfluoride (PMSF) (Beyotime, China). Protein concentration was determined using the BCA protein assay kit (Beyotime, China). Then 10 μg of protein lysis buffer was used for Western Blot assay. In our study, 10% resolving gels were used for SDS-PAGE. The proteins were then transferred to PVDF membranes (Millipore, USA). After blocking with 5% non-fat milk for 2 hours at room temperature, the membranes were incubated with the corresponding primary antibodies for an additional 12 hours at 4°C (PAFAH2, 1:300, SAB, #37205, USA; β-actin, 1:2000, Proteintech, #60008-1-Ig, China). Following 4 times of being washed with TBST, the membranes were incubated with HRP-conjugated secondary antibody (1:2500, Proteintech, #SA00001-2, China) for 2 hours at room temperature. Finally, ECL reagents (Millipore, USA) were used to visualize proteins on membranes.

Paraffin-embedded tissue slides of ccRCC were stained using an immunohistochemical detection kit (Absin, China). The primary antibody to PAFAH2 was diluted 1:200 (SAB, #37205, USA).

CCK-8 and EDU assays

The CCK-8 Cell Counting Kit (Vazyme Biotech, China) and BeyoClick™ EdU Cell Proliferation Kit with Alexa Fluor 555 (Beyotime, China) were used to measure the proliferation ability of ccRCC cells. For CCK-8 assays, 100 ul of medium containing $2*10^3$ cells was added to each well of a 96-well plate. Before measuring, the medium in the wells to be tested was replaced with fresh medium containing 10% CCK-8, and then placed in an incubator for 2 hours. Then a microplate reader was used to measure the OD of the wells to be tested at a wavelength of 450 nm.

For EDU assays, $2*10^4$ cells per well of a 24-well plate were incubated in a 37°C, 5% CO_2 incubator for 22 hours, then incubated with 1X EDU solution for 2 hours. Afterwards, cells were fixed, reacted, stained, and photographed according to standard protocols.

Transwell and wound healing assays

For transwell assays, $2*10^4$ cells transfected with si-PAFAH2 for 48 hours were injected into a transwell chamber containing serum-free medium. RPMI-1640 containing 10% FBS was added to the bottom of the chamber. The chambers were then placed in a 37°C incubator with 5% CO_2 for 24 hours. Then, the migrated

Table 1. Clinical information of included patients

Clinical parameters	Variables	TCGA cohort	GEO cohort	ArrayExpress cohort
Survival status	Dead	145	16	23
	Alive	275	23	78
Age (years)	< 65	262	20	52
	> 65 or = 65	158	19	49
Gender	Male	277	NR	77
	Female	143	NR	24
	NR	0	39	0
Pathology stage	I	215	NR	NR
	II	44	NR	NR
	III	95	NR	NR
	IV	66	NR	NR
	NR	0	39	101
Histological grade	G1	7	NR	13
	G2	185	NR	59
	G3	164	NR	22
	G4	57	NR	5
	GX	5	NR	0
	NR	2	39	2

Abbreviations: NR, not recorded.

cells in the chambers were fixed, stained, and counted.

For wound healing assays, cells transfected with si-PAFAH2 for 48 hours were transferred to a 6-well plate. When the cells covered the entire well, a 200 ul sterile pipette tip was used for trace labeling, and the medium was replaced with fresh serum-free medium. Photographs were then taken at 0 hours and 16 hours.

Statistical analysis

Statistical analyses of all data were completed by R software (version 3.5.1, https://www.r-project.org/), SPSS 20.0 (IBM), and PRISM 8.0 (GraphPad software). When the difference met a joint satisfaction of FDR < 0.05 and |log2fold changes (FC)| > 1, it was regarded to be statistically significant. Student's t test was used for continuous variables, while categorical variables were compared with the chi-square (χ^2) test. Wilcoxon rank-sum test was utilized to compare ranked data with two categories. One-way ANOVA was used to analyze CCK-8 assay results. The Pearson coefficient was used to assess the correlation between two continuous variables. The Kruskal-Wallis test was utilized for comparisons among three or more groups. If AUC > 0.60, the model was considered to have certain predictive value. If AUC > 0.75, the prediction model was considered to have good predictive value. All statistical tests were two-sided and $P < 0.05$ was statistically significant.

Results

Construction a prognostic model index based on differentially expressed prognostic MGs

The transcriptome profiling data of 446 ccRCC tissues and 63 normal kidney tissues were downloaded from TCGA database. Then, mRNA expression data of 39 ccRCC patients from the GSE29609 dataset were combined with the TCGA cohort.

After correcting and normalizing the data, we obtained the differentially expressed gene profile between the ccRCC group and the normal group through the "Limma" package. Then, 479 differentially expressed MGs were identified, including 196 up-regulated genes and 283 down-regulated genes (Figure S1A, S1B). By univariate Cox regression analysis, a total of 187 differentially expressed MGs were considered as prognostic MGs. A PPI network was plotted to display the top 30 most associated proteins (Figure S2A). Six clusters were identified by MCODE, and the top 2 clusters with high connectivity were shown in Figure S2B, S2C.

To construct a prognostic model index, the patients in TCGA database were divided into a training cohort and a testing cohort. The patients in TCGA database and the patients in GEO database were merged as the entire cohort.

After excluding patients with a follow-up survival time of less than 90 days (n = 15) and excluding patients with incomplete clinical information (n = 11), we divided the remaining TCGA-ccRCC patients into two groups with similar composition ratios (296 patients for training cohort, 124 patients for testing cohort). **Table 1** shows the clinical characteristics of patients included in the study.

Immediately afterwards, the lasso regression and the multivariate Cox regression analysis were performed in the training cohort to identify key risk genes (Figure S1C, S1D). Finally, four optimal risk genes (P4HA3, PAFAH2, ALAD, and ETNK2) were identified as key risk genes. Among these 4 risk genes, P4HA3 was considered as predictors of poor prognosis. The higher the expression of P4HA3, the worse the prognosis of patients. Three other genes, ETNK2, PAFAH2, and ALAD, were protective factors. According to the results of multivariate Cox regression analysis, we obtained the risk coefficient of these 4 risk genes and then constructed a prognostic model index. The 4 prognostic MGs related PI formula was as follows: (P4HA3 expression) * (0.07090771) + (ETNK2 expression) * (-0.0497429) + (PAFAH2 expression) * (-0.1753559) + (ALAD expression) * (-0.0880467).

Evaluation of the prognostic model index in the training cohort and the testing cohort

First, the expression differences of the risk genes at the protein level were validated in the HPA database (Figure S1E). This indicates that our model is credible to a certain extent.

Then, we plotted K-M curves based on the log-rank test to visualize the prognostic value of our model in the training cohort and in the testing cohort (Figures S3A, S4A). We found that whether in the training cohort or in the testing cohort, patients in the high-risk group have worse prognosis than those in the low-risk group (HR = 1.1, 95% CI = 1.1-1.2, P < 0.001; HR = 1.1, 95% CI = 1.1-1.2, P < 0.001). Figures S3B and S4B respectively show the time-dependent ROC curves of *riskScore* in predicting the prognosis of training cohort patients and testing cohort patients. In the training cohort, the AUC of the prognostic model at 1 year, 3 years, and 5 years were 0.709, 0.719, and 0.708 respectively. In the testing cohort, the AUC of the prognostic model at 1 year, 3 years, and 5 years were 0.781, 0.769, and 0.703 respectively. In addition, DCA analysis also demonstrated that *riskScore* showed the best net beneft for overall survival (Figures S3C, S4C). Figures S3D and S4D show the results of risk classification of patients in the training cohort and in the testing cohort according to *riskScore* respectively. From Figures S3E and S4E, we found that as the risk score increases, the number of dead patients increases. The expression patterns of the risk genes in the high-risk group and the low-risk group are shown in Figures S3F and S4F, from which we found that whether in the training cohort or in the testing cohort, P4HA3 was up-regulated in the high-risk group, down-regulated in the low-risk group. The expression patterns of ETNK2, PAFAH2, and ALAD were opposite.

Evaluation of the prognostic model index in the entire cohort

Figure 1 shows the preliminary validation results of the performance of the prognostic model in all patients. A K-M curve, a DCA curve, and a ROC curve of multiple prognostic indicators were created to visualize the prognostic value of our model in the entire cohort (**Figure 1A-E**). The overall survival rate of ccRCC patients in the low-risk group was significantly better than that in the high-risk group (HR = 1.1, 95% CI = 1.1-1.2, P < 0.001, **Figure 1A**). DCA suggested that within the risk threshold range of 0.21-0.73, *riskScore* showed the best net benefit compared to age, stage, and grade (**Figure 1B**). In addition, the AUC of the prognostic model at 3 year, 5 years, and 10 years were 0.757, 0.803, and 0.894 respectively, while the AUC of stage at 1, 3, and 5 years was 0.761, 0.712, and 0.641, respectively (**Figure 1C-E**). **Figure 1F** shows the result of risk classification of patients according to *riskScore*. **Figure 1G** shows as the risk score increases, the number of deaths increases. The expression patterns of the risk genes in the high-risk group and the low-risk group are shown in **Figure 1H**.

Evaluation of the prognostic model index in the ArrayExpress cohort

To verify whether our model was reliable, we evaluated the prognostic value of *riskScore* in the external cohort from ArrayExpress database (E-MTAB-1980). The external cohort contained 101 patients with ccRCC. Similarly, we calculated the risk score of each patient based on *riskScore*. Then we divided the patients into a high-risk group and a low-risk group according to the cutoff value we obtained in the training cohort. A K-M curve and a time-depedent ROC curve were created (**Figure 2A** and **2B**). The AUC values of *riskScore* were 0.763 for 1-year-OS, 0.808 for 3-year-OS, and 0.752 for 5-year-OS. In addition, we further investigated

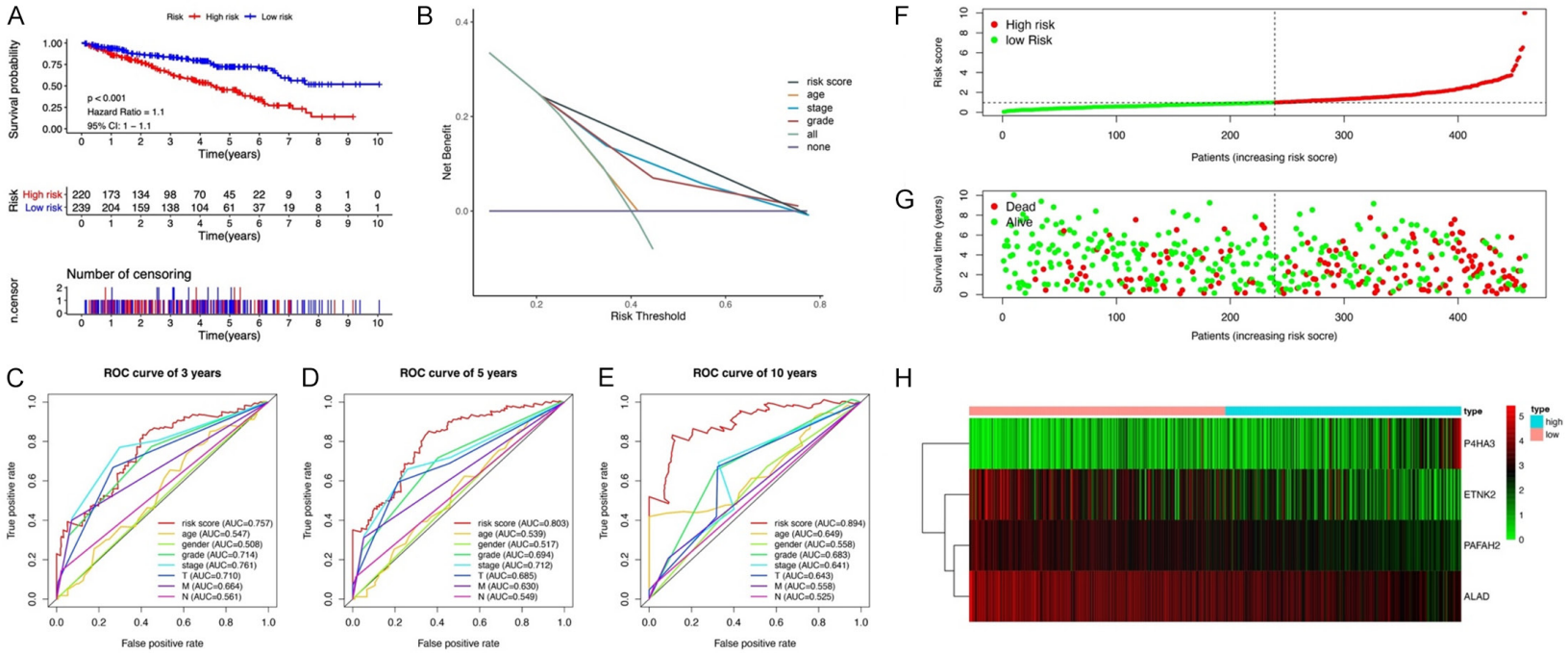

Figure 1. Prognostic analysis of the prognostic model in entire cohort. A. Kaplan-Meier curve analysis of the high-risk and low-risk groups. B. DCA analysis of different variables in the TCGA cohort. C. ROC curve analysis of different variables in the TCGA cohort at three years. D. ROC curve analysis of different variables in the TCGA cohort at five years. E. ROC curve analysis of different variables in the TCGA cohort at ten years. F. Risk score distribution of patients in the prognostic model. G. Survival status scatter plots for patients in the prognostic model. H. Expression patterns of risk genes in the prognostic model.

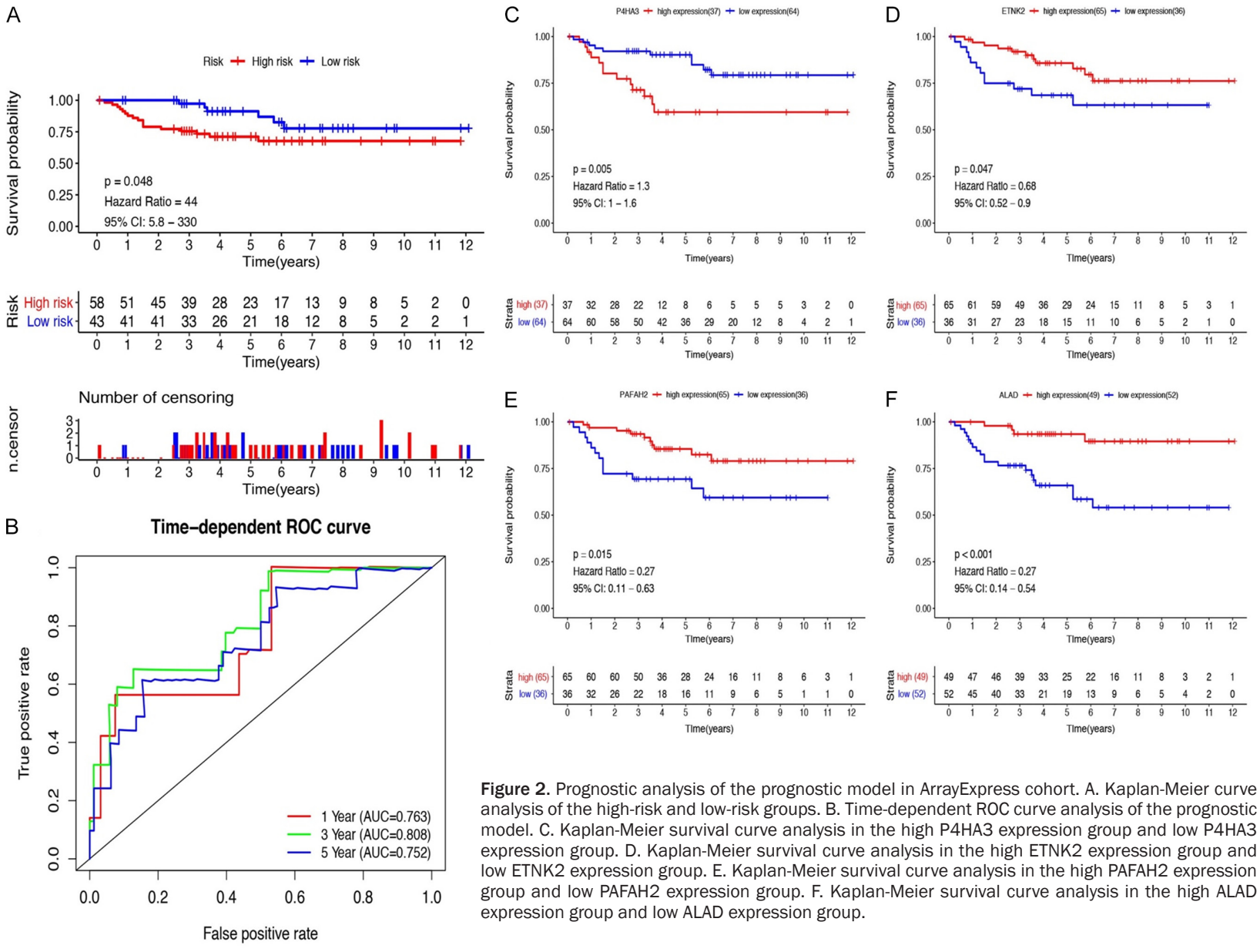

Figure 2. Prognostic analysis of the prognostic model in ArrayExpress cohort. A. Kaplan-Meier curve analysis of the high-risk and low-risk groups. B. Time-dependent ROC curve analysis of the prognostic model. C. Kaplan-Meier survival curve analysis in the high P4HA3 expression group and low P4HA3 expression group. D. Kaplan-Meier survival curve analysis in the high ETNK2 expression group and low ETNK2 expression group. E. Kaplan-Meier survival curve analysis in the high PAFAH2 expression group and low PAFAH2 expression group. F. Kaplan-Meier survival curve analysis in the high ALAD expression group and low ALAD expression group.

whether each risk gene is related to the prognosis of ccRCC. **Figure 2C-F** show that risk genes are significantly related to prognosis. Among them, the higher the expression of P4HA3, the worse the prognosis of patients. ETNK2, PAFAH2, and ALAD all show the role of protective prognostic factors, which is consistent with the conclusions we have obtained before.

Clinical correlation analysis

Based on the information of all ccRCC patients from TCGA database, the correlation between risk factors in the prognostic model (*riskScore* and each component gene) and clinical characteristics such as age, gender, pathology stage, histological grade, and TMN was analyzed. **Figure 3** shows that *riskScore* was significantly correlated with gender, pathology stage, histological grade, T, and M (**Figure 3A**).

Independent prognostic factor evaluation

To further evaluate whether our model could be used as an independent prognostic factor, we included some key clinical characteristics containing age, gender, pathology stage, histological grade, TMN, and *riskScore* as independent variables. Our model showed significant prognostic value in both univariate and multivariate cox regression analyses (both $P < 0.001$, **Table 2**). In addition, the results of multivariate Cox regression analysis also showed that histological grade and M could be used as independent prognostic indicators (both $P < 0.05$).

Nomogram development and validation

To better predict the 1-year OS, 3-year OS, and 5-year OS of ccRCC patients, we constructed a new Nomogram based on the results of the multivariate Cox regression analysis of independent prognostic factors (**Figure 4A**). The C-index of the nomogram for OS prediction was 0.763 (95% CI = 0.701-0.825), while the C-index of *riskScore* for OS prediction was 0.722 (95% CI = 0.659-0.785) (**Figure 4B**). **Figure 4C** shows the Calibration curves of the nomogram for the probability of OS at 1, 3, and 5 year.

Function enrichment analysis and exploration of immune landscape

To further explore the possible mechanisms that caused different outcomes in the high-risk group and the low-risk group, GO enrichment analysis and GSEA were performed. GO enrichment indicated that the differential genes between the two groups were enriched in some humoral immunity-related GO terms (**Figure 5A**). **Figure 5B** plots enriched pathways in the high-risk group, while **Figure 5C** plots enriched pathways in the low-risk group. The results of GSEA suggested that most of the differentially expressed genes in the low-risk group were genes related to metabolic pathways. These results indicate that *riskScore* can not only reflect the situation of metabolic pathways, but may also be related to some tumor immune events.

In addition, we explored the relationship between *riskScore* and some immune-related activities. We found that chemokine receptors (CCR), parainflammation, MHC class I, immune checkpoints, T cell co-stimulation, cytolytic activity, and inflammation-promoting were significantly different between high-risk group and low-risk group (**Figure 5D**). Meanwhile, no significant differences in somatic mutations were observed between high-risk group and low-risk group (**Figure 5E**). CIBERSORT results showed that activated memory CD4+ T Cells, regulatory T cells (Tregs), and M0 Macrophages were highly expressed in the high-risk group, while Monocytes, M1 Macrophages, M2 Macrophages, resting Dendritic cells, and resting Mast cells were highly expressed in the low-risk group (**Figure 5F**). Correlation analysis showed that *riskScore* was positively correlated with activated memory CD4+ T Cells, Tregs, and M0 Macrophages, and negatively correlated with Monocytes, M1 Macrophages, M2 Macrophages, resting Dendritic cells, and resting Mast cells (**Figure 5G**). Besides, patients in the high-risk group had significantly higher TIDE scores than those in the low-risk group (**Figure 5H**).

Drug sensitivity prediction

To explore whether *riskScore* can guide the selection of treatment strategies for patients, we used the GDSC database to predict the response of different subgroups to 8 common targeted drugs (Figure S5). A total of 3 targeted drugs showed a significant difference in IC50 between high-risk and low-risk groups (Sunitinib, Axitinib, and Lapatinib).

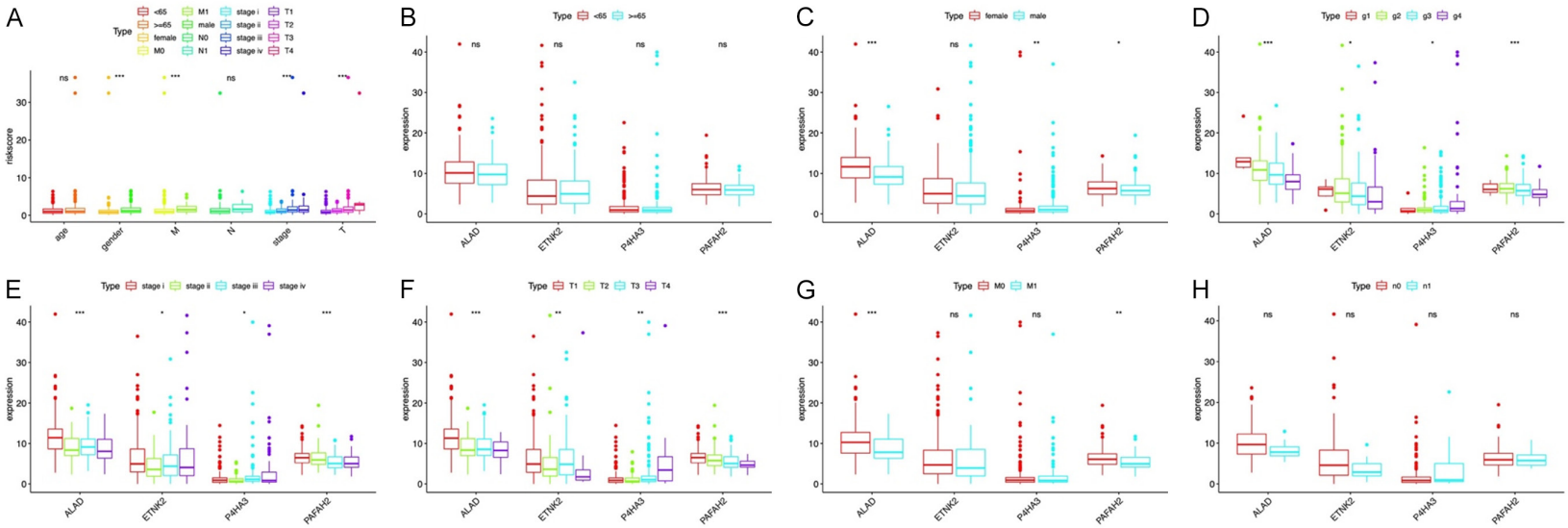

Figure 3. Relationships of the variables in the model with the clinical characteristics of patients in the TCGA cohort. A. *riskScore* and clinical variables. B. Expression of risk genes and age. C. Expression of risk genes and gender. D. Expression of risk genes and grade. E. Expression of risk genes and stage. F. Expression of risk genes and T. G. Expression of risk genes and M. H. Expression of risk genes and N. Abbreviations: *, $P < 0.05$; **, $P < 0.01$; ***, $P < 0.001$.

Table 2. Univariate and multivariate cox regression analyses of OS in the TCGA cohort

Variables	Univariate Cox		Multivariate Cox	
	Hazard ratio (95% CI)	*P* value	Hazard ratio (95% CI)	*P* value
Age	1.014 (0.996-1.032)	0.132	1.027 (1.005-1.049)	0.015
Gender	1.168 (0.728-1.876)	0.519	1.667 (0.978-2.842)	0.060
Histological grade	2.336 (1.692-3.226)	< 0.001	1.497 (1.017-2.204)	0.041
Pathological stage	1.831 (1.488-2.254)	< 0.001	1.029 (0.520-2.039)	0.934
T	1.952 (1.508-2.527)	< 0.001	1.164 (0.595-2.278)	0.658
M	4.382 (2.670-7.192)	< 0.001	3.811 (1.314-11.054)	0.014
N	2.701 (1.235-5.908)	0.013	1.503 (0.373-2.972)	0.922
Riskscore	1.134 (1.085-1.184)	< 0.001	1.114 (1.053-1.179)	< 0.001

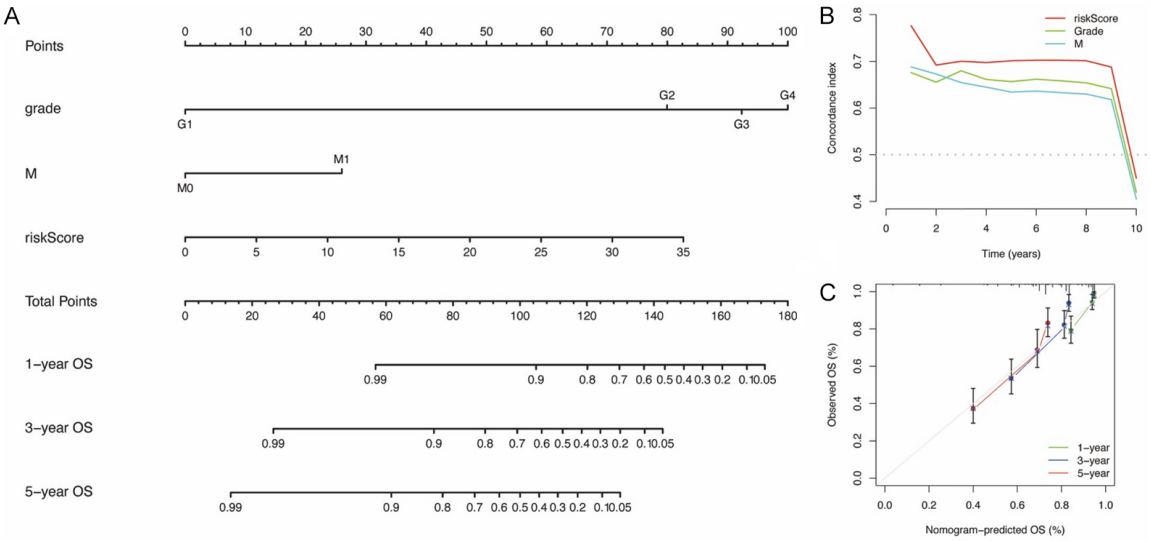

Figure 4. Nomogram for the predictions of prognosis at one, three, and five years in the TCGA cohort. A. Nomogram for OS. B. Concordance index of the prognostic predictions. C. Calibration curves at 1, 3, and 5 years.

The role of PAFAH2 in ccRCC

Among the 4 key MGs, PAFAH2 (with the highest weight coefficient) was selected for further functional exploration. Firstly, we verified that the mRNA level of PAFAH2 is downregulated in cancer tissues (**Figure 6A**). At the protein expression level, CPTAC database analysis, Western Blot, and IHC results indicated that PAFAH2 was down-regulated in cancer tissues (**Figure 6B-D**).

To reveal the function of PAFAH2 in ccRCC cells, we knocked down PAFAH2 in ccRCC cells by transfecting siRNAs. **Figure 6E** shows that mRNA levels of PAFAH2 were reduced by 60%-70% in 786-O cells. Western Blot also yielded consistent results (**Figure 6F**). The proliferation ability of 786-O cells and 769-P cells was significantly improved after knockdown of PAFAH2 (**Figure 6G**, **6H**). Similar results were obtained in Edu assays (**Figure 6I**, **6J**). In addition, compared with negative control cells, 786-O cells and 769-P cells migrated more easily after knockdown of PAFAH2. This phenomenon was confirmed in transwell assays and wound healing assays (**Figure 6K-M**).

Discussion

In recent years, the incidence of asymptomatic ccRCC has been increasing. Advanced ccRCC patients are prone to poor prognosis and high mortality, which brings new challenges to early clinical detection and treatment [31]. It is well known that chemotherapy and radiotherapy are not ideal for the treatment of ccRCC. Although targeted drug therapy can inhibit the metasta-

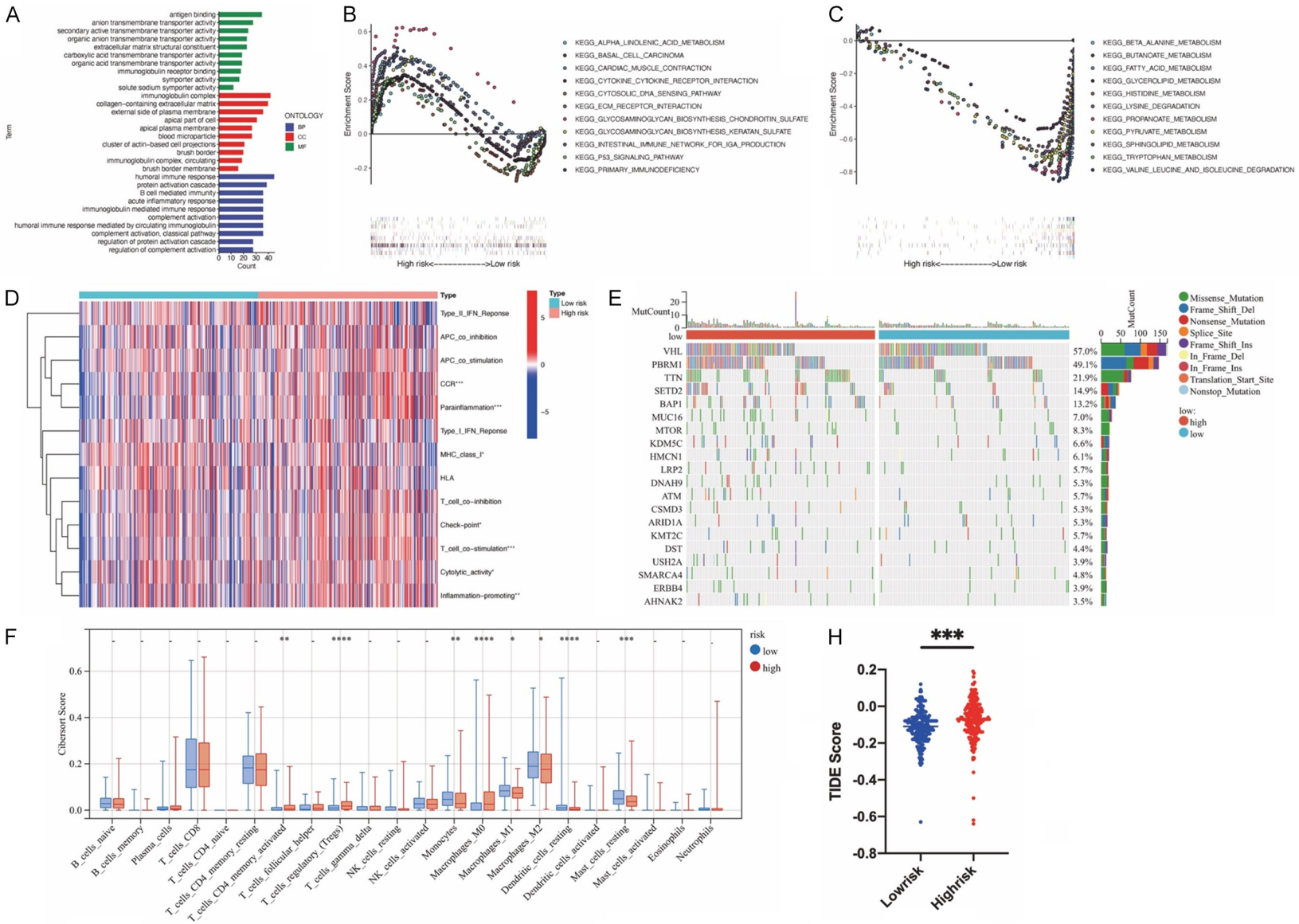
A
antigen binding
anion transmembrane transporter activity
secondary active transmembrane transporter activity
organic anion transmembrane transporter activity
extracellular matrix structural constituent
carboxylic acid transmembrane transporter activity
organic acid transmembrane transporter activity
immunoglobulin receptor binding
symporter activity
solute:sodium symporter activity
immunoglobulin complex
collagen-containing extracellular matrix
external side of plasma membrane
apical part of cell
apical plasma membrane
blood microparticle
cluster of actin-based cell projections
brush border
immunoglobulin complex, circulating
brush border membrane
humoral immune response
protein activation cascade
B cell mediated immunity
acute inflammatory response
immunoglobulin mediated immune response
complement activation
humoral immune response mediated by circulating immunoglobulin
complement activation, classical pathway
regulation of protein activation cascade
regulation of complement activation
Term
Count
ONTOLOGY
BP
CC
MF
B
Enrichment Score
KEGG_ALPHA_LINOLENIC_ACID_METABOLISM
KEGG_BASAL_CELL_CARCINOMA
KEGG_CARDIAC_MUSCLE_CONTRACTION
KEGG_CYTOKINE_CYTOKINE_RECEPTOR_INTERACTION
KEGG_CYTOSOLIC_DNA_SENSING_PATHWAY
KEGG_ECM_RECEPTOR_INTERACTION
KEGG_GLYCOSAMINOGLYCAN_BIOSYNTHESIS_CHONDROITIN_SULFATE
KEGG_GLYCOSAMINOGLYCAN_BIOSYNTHESIS_KERATAN_SULFATE
KEGG_INTESTINAL_IMMUNE_NETWORK_FOR_IGA_PRODUCTION
KEGG_P53_SIGNALING_PATHWAY
KEGG_PRIMARY_IMMUNODEFICIENCY
High risk<---------->Low risk
C
Enrichment Score
KEGG_BETA_ALANINE_METABOLISM
KEGG_BUTANOATE_METABOLISM
KEGG_FATTY_ACID_METABOLISM
KEGG_GLYCEROLIPID_METABOLISM
KEGG_HISTIDINE_METABOLISM
KEGG_LYSINE_DEGRADATION
KEGG_PROPANOATE_METABOLISM
KEGG_PYRUVATE_METABOLISM
KEGG_SPHINGOLIPID_METABOLISM
KEGG_TRYPTOPHAN_METABOLISM
KEGG_VALINE_LEUCINE_AND_ISOLEUCINE_DEGRADATION
High risk<---------->Low risk
D
Type
Type_II_IFN_Reponse
APC_co_inhibition
APC_co_stimulation
CCR***
Parainflammation***
Type_I_IFN_Reponse
MHC_class_I*
HLA
T_cell_co-inhibition
Check-point*
T_cell_co-stimulation***
Cytolytic_activity*
Inflammation-promoting**
Low risk
High risk
E
MutCount
low
VHL 57.0%
PBRM1 49.1%
TTN 21.9%
SETD2 14.9%
BAP1 13.2%
MUC16 7.0%
MTOR 8.3%
KDM5C 6.6%
HMCN1 6.1%
LRP2 5.7%
DNAH9 5.3%
ATM 5.7%
CSMD3 5.3%
ARID1A 5.3%
KMT2C 5.7%
DST 4.4%
USH2A 3.9%
SMARCA4 4.8%
ERBB4 3.9%
AHNAK2 3.5%
Missense_Mutation
Frame_Shift_Del
Nonsense_Mutation
Splice_Site
Frame_Shift_Ins
In_Frame_Del
In_Frame_Ins
Translation_Start_Site
Nonstop_Mutation
low:
high
low
F
Cibersort Score
risk
low
high
B_cells_naive
B_cells_memory
Plasma_cells
T_cells_CD8
T_cells_CD4_naive
T_cells_CD4_memory_resting
T_cells_CD4_memory_activated
T_cells_follicular_helper
T_cells_regulatory_(Tregs)
T_cells_gamma_delta
NK_cells_resting
NK_cells_activated
Monocytes
Macrophages_M0
Macrophages_M1
Macrophages_M2
Dendritic_cells_resting
Dendritic_cells_activated
Mast_cells_resting
Mast_cells_activated
Eosinophils
Neutrophils
H
***
TIDE Score
Lowrisk
Highrisk

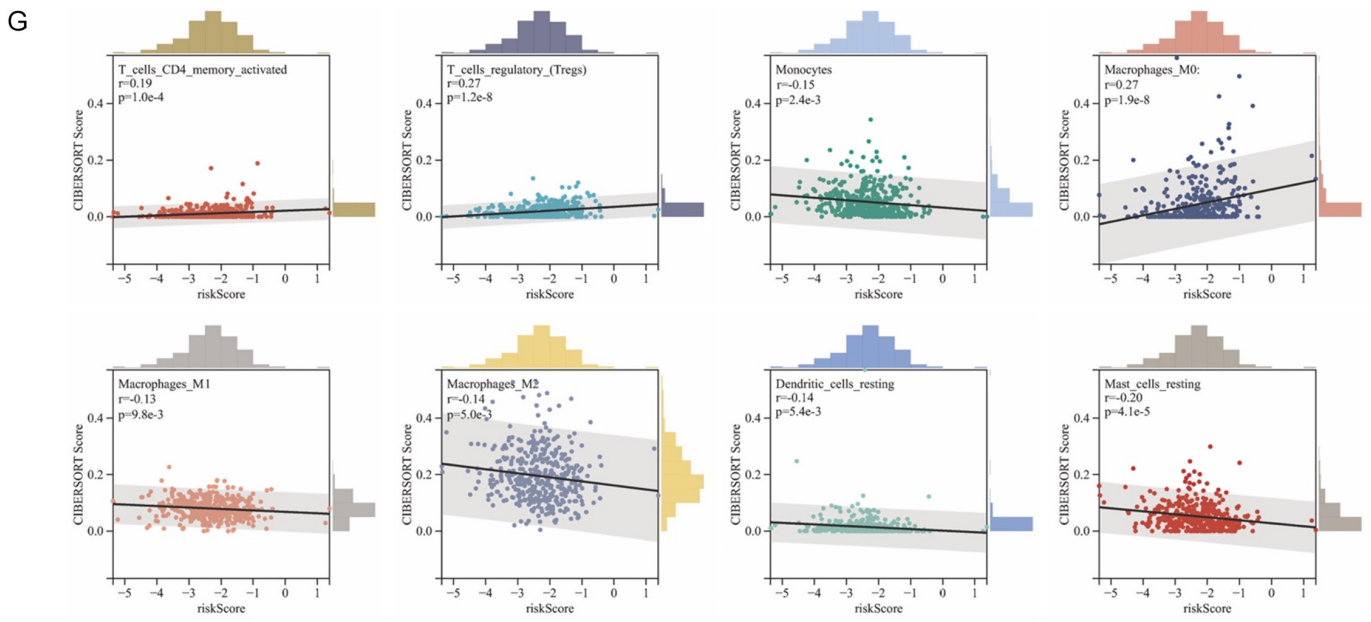

Figure 5. Function enrichment analysis and exploration of immune landscape. A. GO enrichment analysis of genes that are differentially expressed between high-risk and low-risk groups. B. Gene-set enrichment analysis in high-risk group. C. Gene-set enrichment analysis in low-risk group. D. Differences in ssGSEA scores of immune cells and immune function between high-risk and low-risk groups. E. Differences in somatic mutation between high-risk and low-risk groups. F. Differences in immune cell infiltration between high-risk and low-risk groups. G. Immune infiltrating cells significantly correlated with riskScore. H. Differences in TIDE scores between high-risk and low-risk groups. Abbreviations: *, P < 0.05; **, P < 0.01; ***, P < 0.001; ****, P < 0.0001.

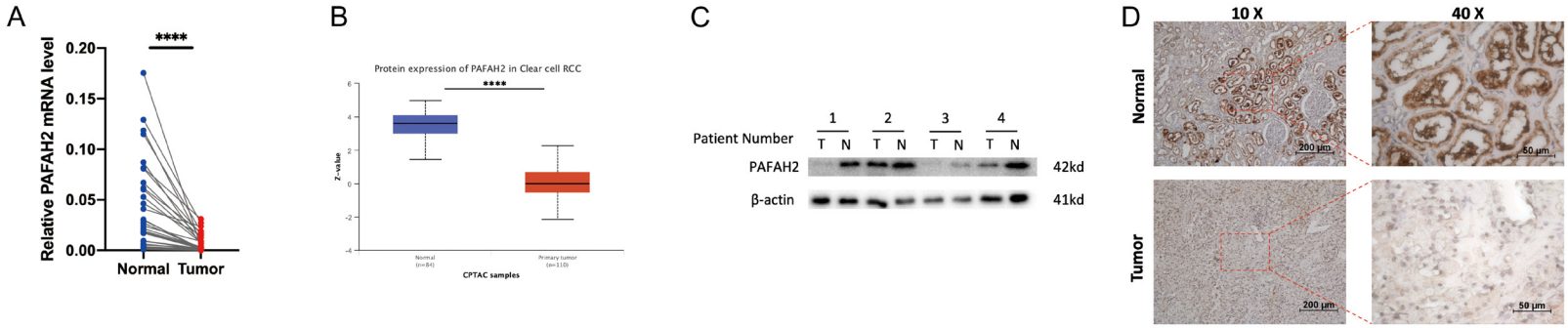

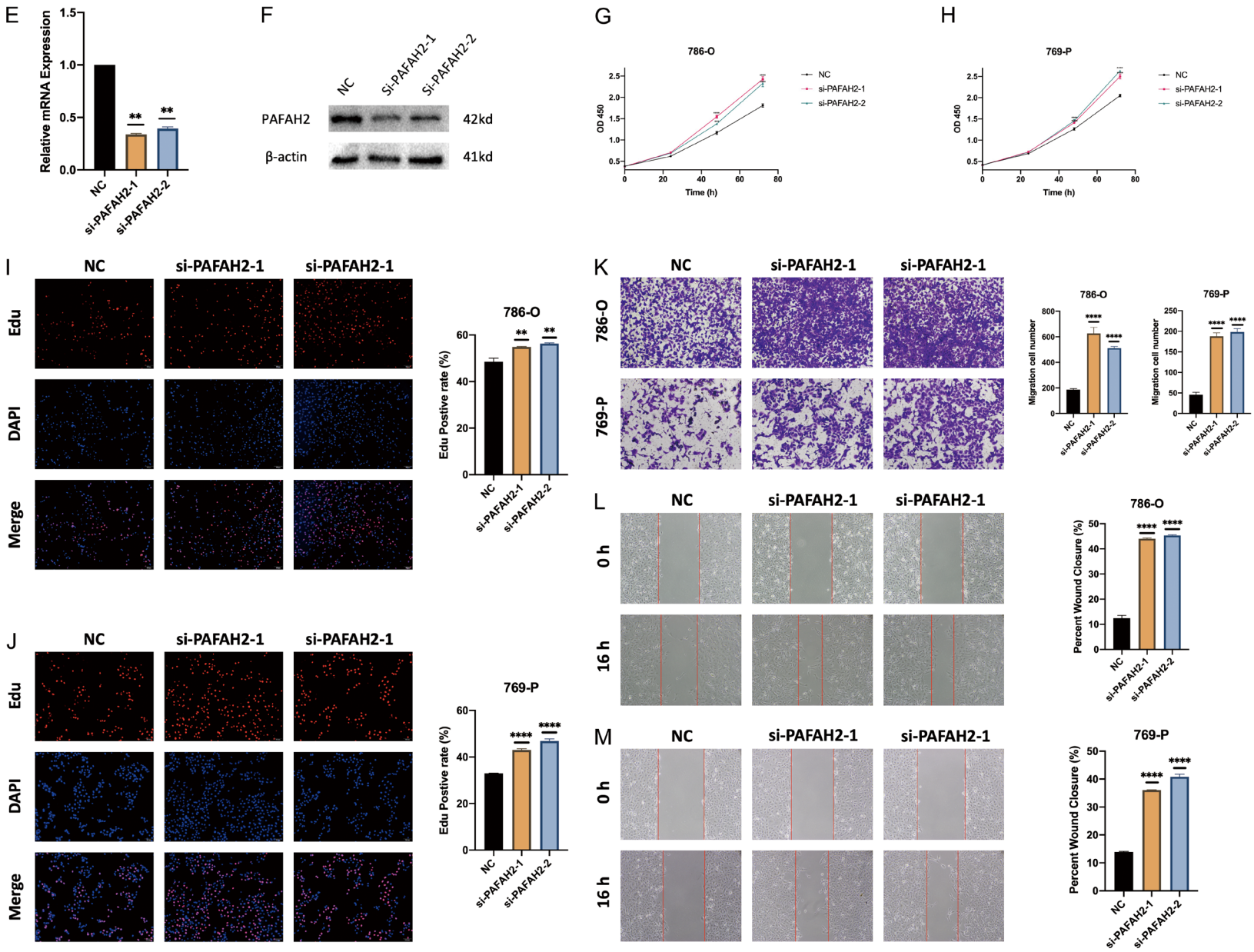
E
Relative mRNA Expression
1.5
1.0
0.5
0.0
**
**
NC
si-PAFAH2-1
si-PAFAH2-2
F
NC
Si-PAFAH2-1
Si-PAFAH2-2
PAFAH2
42kd
β-actin
41kd
G
786-O
OD 450
Time (h)
NC
si-PAFAH2-1
si-PAFAH2-2
H
769-P
OD 450
Time (h)
NC
si-PAFAH2-1
si-PAFAH2-2
I
NC
si-PAFAH2-1
si-PAFAH2-1
Edu
DAPI
Merge
786-O
Edu Postive rate (%)
NC
si-PAFAH2-1
si-PAFAH2-2
J
NC
si-PAFAH2-1
si-PAFAH2-1
Edu
DAPI
Merge
769-P
Edu Postive rate (%)
NC
si-PAFAH2-1
si-PAFAH2-2
K
NC
si-PAFAH2-1
si-PAFAH2-1
786-O
769-P
786-O
Migration cell number
769-P
Migration cell number
L
NC
si-PAFAH2-1
si-PAFAH2-1
0 h
16 h
786-O
Percent Wound Closure (%)
M
NC
si-PAFAH2-1
si-PAFAH2-1
0 h
16 h
769-P
Percent Wound Closure (%)

Figure 6. PAFAH2 is lowly expressed in ccRCC and can inhibit the proliferation and migration of ccRCC cells. (A) Relative mRNA expression levels of PAFAH2 in ccRCC tissues (32 pairs). (B) Protein expression levels of PAFAH2 in ccRCC tissues (CPTAC database). (C) Protein expression levels of PAFAH2 in 4 ccRCC tissues (Western Blot). (D) IHC staining of PAFAH2 protein in ccRCC patient tumors and matched paracancerous tissues. (E, F) The effect of PAFAH2 siRNAs in 786-O cells was assessed by qRT-PCR (E) and Western Blot (F). (G, H) CCK-8 assays showed that knockdown of PAFAH2 levels increased the proliferation of ccRCC cells (G: 786-O, H: 769-P). (I, J) EDU assays suggested that knockdown of PAFAH2 levels increased the proliferation of ccRCC cells (I: 786-O, J: 769-P). (K) Transwell assays indicated that knockdown of PAFAH2 levels increased the migratory ability of ccRCC cells. (L, M) Wound healing assays showed that ccRCC cells with low levels of PAFAH2 moved more rapidly (L: 786-O, M: 769-P). Abbreviations: *, $P < 0.05$; **, $P < 0.01$; ***, $P < 0.001$; ****, $P < 0.0001$.

sis and development of advanced tumors to a certain extent, drug resistance is inevitable [32, 33]. At present, immune checkpoint (PD-1, PD-L1, CTLA4, etc.) inhibitors have been used for the treatment of advanced ccRCC [34, 35]. However, only partial patients can benefit from it [6, 7, 36, 37]. Existing studies have shown that some commonly used predictors, such as tumor mutational burden (TMB), PD-1/PD-L1 expression, and CD8+ T cell infiltration, cannot well predict the response of ccRCC to immune checkpoint inhibitors [38, 39]. Therefore, biological indicators of ccRCC prognosis and immunotherapy response have become the focus of research in recent years [40, 41].

Changes in metabolic pathways exist in many diseases, including tumors. Metabolic reprogramming is very important to maintain abnormal proliferation of tumor cells [42]. More and more cancer researchers are focusing their attention on the mechanism of tumor metabolic changes. A recent study pointed out that the heterogeneity of metabolic reprogramming within tumors is clearly related to the tumor outcome [43]. Novel cancer therapies targeting metabolic pathways are being investigated in many tumors. Mucin 1 (MUC1), a global regulator of glucose metabolism, has recently been identified as a therapeutic target for pancreatic cancer. After knocking out MUC1 in pancreatic cancer cells, Fu et al. found that metabolic activity of the cancer cells was significantly reduced and that cancer cells became more sensitive chemotherapy [44]. Similarly, in soft tissue sarcoma, targeting glutamine metabolism can well inhibit tumor growth [45]. In addition, drugs that inhibit glucose and lipid metabolism can be used to treat lung cancer [46]. Recently, some researchers have considered that ccRCC is a metabolic disease [27]. They suggested that alterations in some metabolic pathways could serve as therapeutic targets and potential biomarkers for diagnosis and prognosis. Lucarelli et al. pointed out that the abnormal expression of MGs is closely related to the occurrence and development of tumors. They further determined that NADH dehydrogenase (ubiquinone) 1 alpha subcomplex 4-like 2 (NDUFA4L2) plays an important role in the occurrence and development of ccRCC [47]. However, few studies have investigated the potential value of MGs in predicting ccRCC prognosis and response to immunotherapy.

In this study, we screened and validated the prognostic MGs of ccRCC from the TCGA, GEO, and ArrayExpress database. Finally, we successfully established a risk model (*riskScore*) based on 4 MGs, which can accurately predict the prognosis of ccRCC. The scientific model construction methods, comprehensive evaluation of prognostic value, and validation in multiple databases make the *riskScore* highly reliable. According to the *riskScore*, patients with different survival outcomes can be accurately distinguished. In addition, GO and GSEA analysis results suggest that the disorder of metabolic pathways and immune-related activities plays a very important role in ccRCC. Whether metabolic disturbances in ccRCC lead to alterations in TME? Recent studies have shown that the TME of ccRCC is closely related to the response to immune checkpoint inhibitors [48, 49]. Therefore, we further explored the relationship between *riskScore* and TME. Our study found that *riskScore* was significantly positively correlated with the infiltration of activated memory CD4+ T Cells, Tregs, and M0 Macrophages. This may be because higher risk scores indicate worse metabolic disorders. Intratumoral metabolic disorders are often accompanied by elevated lactate levels and abnormal chemokine receptor (CCR) expression, leading to the recruitment of macrophages and tregs, and the construction of immunosuppressive TME [28, 50-52]. This also explains why patients in the high-risk group have higher TIDE scores.

P4HA3, ETNK2, PAFAH2, and ALAD are the four risk MGs we identified. Among them, P4HA3 was considered as predictors of poor prognosis. The higher the expression of P4HA3, the worse the prognosis of patients. Three other genes, ETNK2, PAFAH2, and ALAD, were protective factors. P4HA3, encoding a component of prolyl 4-hydroxylase, can catalyze a 4-hydroxylation on prolines in collagen. Studies have shown that P4HA3 can promote the invasion and metastasis of tumors by stabilizing collagen [53]. In melanoma, P4HA3 promotes the proliferation and invasion of melanoma cells [54]. In addition, P4HA3 has been shown to be closely related to the poor survival outcomes of breast cancer and gastric cancer [55, 56]. Therefore, the mechanism of P4HA3 overexpression in the occurrence and development of ccRCC needs further research and exploration. ETNK2 (Ethanolamine Kinase 2) is involved in phosphatidylethanolamine biosynthesis II and Glycerophospholipid biosynthesis. Disorders of phospholipid metabolism have been found to be related to tumor progression in a variety of cancers, including glioblastoma, lung cancer, liver cancer and kidney cancer [57, 58]. The decreased expression of ETNK2 is related to the progression of prostate cancer [59]. PAFAH2 is closely related to ether lipid metabolism. Kono et al. revealed that PAFAH2 is involved in the metabolism of esterified 8-isoprostaglandin F (2alpha) and protects tissue from oxidative stress-induced injury [60]. However, the relationship between PAFAH2 and the prognosis of ccRCC remains unclear. This research suggests that high expression of PAFAH2 is associated with better prognosis in ccRCC. Experiments in vitro (786-0 cells and 769-P cells) also showed that PAFAH2 has a tumor suppressor effect. ALAD Catalyzes an early step in the biosynthesis of tetrapyrroles. ALAD has been found to be related to the favorable survival outcome of breast cancer patients. Overexpression of ALAD can inhibit the proliferation and invasion of breast cancer cells [61].

This research suggests that changes in the expression of some MGs are closely related to the prognosis, and TME of ccRCCs. Considering that alterations in metabolic pathways and MGs play important roles in the occurrence, development, and prognosis of ccRCC, we wondered whether some metabolic biomarkers can be used to improve the early diagnosis rate of ccRCC, which requires further research to explore. In addition, our research also sheds new light on the treatment of ccRCC.

However, our study still has some limitations: The results of our study were only validated in the TCGA, GEO, and ArrayExpress database. More data support from clinical patients is needed. In addition, the mechanism by which MGs affect the prognosis of patients with ccRCC needs to be further explored through in vivo and in vitro experiments.

Conclusions

All in all, we have successfully established a risk model (*riskScore*) based on 4 MGs, which could accurately predict the prognosis of ccRCCs and help to screen patients suitable for immune checkpoint inhibitors therapy. We also preliminarily verified the tumor suppressor effect of the key gene PAFAH2 in ccRCC. Our research may shed new light on ccRCC patients' prognosis and treatment management. However, further experiments are also required to validate our findings.

Acknowledgements

We would like to thank the researchers and study participants for their contributions. This article was funded by the National Natural Science Foundation of China (grant number: 81871151, 82071638, and 82103580).

Patients in this study provided written informed consent to participate in this study.

Disclosure of conflict of interest

None.

Abbreviations

RCC, Renal cell carcinoma; ccRCC, Clear cell renal cell carcinoma; TCGA, The Cancer Genome Atlas; GEO, Gene Expression Omnibus; HPA, The Human Protein Atlas; DEGs, Differentially expressed genes; MGs, Metabolic genes; PI, Prognostic index; KEGG, Kyoto Encyclopedia of Genes and Genomes; ROC, Receiver operating characteristic; AUC, Area under the curve; DCA, Decision curve analysis; OS, Overall survival; K-M, Kaplan-Meier; FC, Fold change; LASSO, Least absolute shrinkage and selection operator; IHC, Immunohistochemistry; HR, Hazard ratio; CI, Confidence interval.

Address correspondence to: Ning-Hong Song, Department of Urology, The First Affiliated Hospital of Nanjing Medical University, No. 300 Guangzhou Road, Nanjing 210029, Jiangsu, China. Tel: +86-13851490672; E-mail: songninghong_urol@163.com

References

[1] Siegel RL, Miller KD and Jemal A. Cancer statistics, 2019. CA Cancer J Clin 2019; 69: 7-34.

[2] Hakimi AA, Voss MH, Kuo F, Sanchez A, Liu M, Nixon BG, Vuong L, Ostrovnaya I, Chen YB, Reuter V, Riaz N, Cheng Y, Patel P, Marker M, Reising A, Li MO, Chan TA and Motzer RJ. Transcriptomic profiling of the tumor microenvironment reveals distinct subgroups of clear cell renal cell cancer: data from a randomized phase III trial. Cancer Discov 2019; 9: 510-525.

[3] Rossi SH, Klatte T, Usher-Smith J and Stewart GD. Epidemiology and screening for renal cancer. World J Urol 2018; 36: 1341-1353.

[4] Choueiri TK and Motzer RJ. Systemic therapy for metastatic renal-cell carcinoma. N Engl J Med 2017; 376: 354-366.

[5] Capitanio U and Montorsi F. Renal cancer. Lancet 2016; 387: 894-906.

[6] Rini BI, Plimack ER, Stus V, Gafanov R, Hawkins R, Nosov D, Pouliot F, Alekseev B, Soulières D, Melichar B, Vynnychenko I, Kryzhanivska A, Bondarenko I, Azevedo SJ, Borchiellini D, Szczylik C, Markus M, McDermott RS, Bedke J, Tartas S, Chang YH, Tamada S, Shou Q, Perini RF, Chen M, Atkins MB and Powles T; KEYNOTE-426 Investigators. Pembrolizumab plus axitinib versus sunitinib for advanced renal-cell carcinoma. N Engl J Med 2019; 380: 1116-1127.

[7] Motzer RJ, Penkov K, Haanen J, Rini B, Albiges L, Campbell MT, Venugopal B, Kollmannsberger C, Negrier S, Uemura M, Lee JL, Vasiliev A, Miller WH Jr, Gurney H, Schmidinger M, Larkin J, Atkins MB, Bedke J, Alekseev B, Wang J, Mariani M, Robbins PB, Chudnovsky A, Fowst C, Hariharan S, Huang B, di Pietro A and Choueiri TK. Avelumab plus axitinib versus sunitinib for advanced renal-cell carcinoma. N Engl J Med 2019; 380: 1103-1115.

[8] Chevrier S, Levine JH, Zanotelli VRT, Silina K, Schulz D, Bacac M, Ries CH, Ailles L, Jewett MAS, Moch H, van den Broek M, Beisel C, Stadler MB, Gedye C, Reis B, Pe'er D and Bodenmiller B. An immune atlas of clear cell renal cell carcinoma. Cell 2017; 169: 736-749, e18.

[9] Kreuzaler P, Panina Y, Segal J and Yuneva M. Adapt and conquer: metabolic flexibility in cancer growth, invasion and evasion. Mol Metab 2020; 33: 83-101.

[10] Woolbright BL, Rajendran G, Harris RA and Taylor JA 3rd. Metabolic flexibility in cancer: targeting the pyruvate dehydrogenase kinase: pyruvate dehydrogenase axis. Mol Cancer Ther 2019; 18: 1673-1681.

[11] El Hassouni B, Granchi C, Valles-Marti A, Supadmanaba IGP, Bononi G, Tuccinardi T, Funel N, Jimenez CR, Peters GJ, Giovannetti E and Minutolo F. The dichotomous role of the glycolytic metabolism pathway in cancer metastasis: interplay with the complex tumor microenvironment and novel therapeutic strategies. Semin Cancer Biol 2020; 60: 238-248.

[12] da Costa IA, Hennenlotter J, Stuhler V, Kuhs U, Scharpf M, Todenhofer T, Stenzl A and Bedke J. Transketolase like 1 (TKTL1) expression alterations in prostate cancer tumorigenesis. Urol Oncol 2018; 36: 472.e21-472.e27.

[13] Meng Y, Xu X, Luan H, Li L, Dai W, Li Z and Bian J. The progress and development of GLUT1 inhibitors targeting cancer energy metabolism. Future Med Chem 2019; 11: 2333-2352.

[14] Qiu C, Zhang Y and Chen L. Impaired metabolic pathways related to colorectal cancer progression and therapeutic implications. Iran J Public Health 2020; 49: 56-67.

[15] Trilla-Fuertes L, Gamez-Pozo A, Lopez-Camacho E, Prado-Vazquez G, Zapater-Moros A, Lopez-Vacas R, Arevalillo JM, Diaz-Almiron M, Navarro H, Main P, Espinosa E, Zamora P and Fresno Vara JA. Computational models applied to metabolomics data hints at the relevance of glutamine metabolism in breast cancer. BMC Cancer 2020; 20: 307.

[16] Marin-Rubio JL, Vela-Martin L, Fernandez-Piqueras J and Villa-Morales M. FADD in cancer: mechanisms of altered expression and function, and clinical implications. Cancers (Basel) 2019; 11: 1462.

[17] Roberto D, Selvarajah S, Park PC, Berman D and Venkateswaran V. Functional validation of metabolic genes that distinguish Gleason 3 from Gleason 4 prostate cancer foci. Prostate 2019; 79: 1777-1788.

[18] Zhang S, Lu Y, Liu Z, Li X, Wang Z and Cai Z. Identification six metabolic genes as potential biomarkers for lung adenocarcinoma. J Comput Biol 2020; 27: 1532-1543.

[19] Liu GM, Xie WX, Zhang CY and Xu JW. Identification of a four-gene metabolic signature predicting overall survival for hepatocellular carcinoma. J Cell Physiol 2020; 235: 1624-1636.

[20] Xing L, Guo M, Zhang X, Zhang X and Liu F. A transcriptional metabolic gene-set based prognostic signature is associated with clinical and mutational features in head and neck squamous cell carcinoma. J Cancer Res Clin Oncol 2020; 146: 621-630.

[21] Zhang ZY, Yao QZ, Liu HY, Guo QN, Qiu PJ, Chen JP and Lin JQ. Metabolic reprogramming-asso-

ciated genes predict overall survival for rectal cancer. J Cell Mol Med 2020; 24: 5842-5849.
[22] Gossage L, Eisen T and Maher ER. VHL, the story of a tumour suppressor gene. Nat Rev Cancer 2015; 15: 55-64.
[23] Hsieh JJ, Purdue MP, Signoretti S, Swanton C, Albiges L, Schmidinger M, Heng DY, Larkin J and Ficarra V. Renal cell carcinoma. Nat Rev Dis Primers 2017; 3: 17009.
[24] Bacigalupa ZA and Rathmell WK. Beyond glycolysis: hypoxia signaling as a master regulator of alternative metabolic pathways and the implications in clear cell renal cell carcinoma. Cancer Lett 2020; 489: 19-28.
[25] Yu Y, Yu Q and Zhang X. Allosteric inhibition of HIF-2α as a novel therapy for clear cell renal cell carcinoma. Drug Discov Today 2019; 24: 2332-2340.
[26] Wettersten HI, Aboud OA, Lara PN Jr and Weiss RH. Metabolic reprogramming in clear cell renal cell carcinoma. Nat Rev Nephrol 2017; 13: 410-419.
[27] Lucarelli G, Loizzo D, Franzin R, Battaglia S, Ferro M, Cantiello F, Castellano G, Bettocchi C, Ditonno P and Battaglia M. Metabolomic insights into pathophysiological mechanisms and biomarker discovery in clear cell renal cell carcinoma. Expert Rev Mol Diagn 2019; 19: 397-407.
[28] Fu Q, Xu L, Wang Y, Jiang Q, Liu Z, Zhang J, Zhou Q, Zeng H, Tong S, Wang T, Qi Y, Hu B, Fu H, Xie H, Zhou L, Chang Y, Zhu Y, Dai B, Zhang W and Xu J. Tumor-associated macrophage-derived interleukin-23 interlinks kidney cancer glutamine addiction with immune evasion. Eur Urol 2019; 75: 752-763.
[29] Newman AM, Liu CL, Green MR, Gentles AJ, Feng W, Xu Y, Hoang CD, Diehn M and Alizadeh AA. Robust enumeration of cell subsets from tissue expression profiles. Nat Methods 2015; 12: 453-457.
[30] Fu J, Li K, Zhang W, Wan C, Zhang J, Jiang P and Liu XS. Large-scale public data reuse to model immunotherapy response and resistance. Genome Med 2020; 12: 21.
[31] Sung H, Ferlay J, Siegel RL, Laversanne M, Soerjomataram I, Jemal A and Bray F. Global cancer statistics 2020: GLOBOCAN estimates of incidence and mortality worldwide for 36 cancers in 185 countries. CA Cancer J Clin 2021; 71: 209-249.
[32] Ljungberg B, Bensalah K, Canfield S, Dabestani S, Hofmann F, Hora M, Kuczyk MA, Lam T, Marconi L, Merseburger AS, Mulders P, Powles T, Staehler M, Volpe A and Bex A. EAU guidelines on renal cell carcinoma: 2014 update. Eur Urol 2015; 67: 913-924.
[33] Molina AM, Lin X, Korytowsky B, Matczak E, Lechuga MJ, Wiltshire R and Motzer RJ. Sunitinib objective response in metastatic renal cell carcinoma: analysis of 1059 patients treated on clinical trials. Eur J Cancer 2014; 50: 351-358.
[34] Bedke J, Albiges L, Capitanio U, Giles RH, Hora M, Lam TB, Ljungberg B, Marconi L, Klatte T, Volpe A, Abu-Ghanem Y, Dabestani S, Pello SF, Hofmann F, Kuusk T, Tahbaz R, Powles T and Bex A. The 2021 updated european association of urology guidelines on renal cell carcinoma: immune checkpoint inhibitor-based combination therapies for treatment-naive metastatic clear-cell renal cell carcinoma are standard of care. Eur Urol 2021; 80: 393-397.
[35] Zhuang TZ, Case K, Olsen TA, Brown JT, Carthon BC, Kucuk O, Goldman J, Harris W, Bilen MA and Nazha B. Metastatic clear-cell renal cell carcinoma in the era of immune checkpoint inhibitors: therapies and ongoing trials. Cancers (Basel) 2022; 14: 2867.
[36] Motzer R, Alekseev B, Rha SY, Porta C, Eto M, Powles T, Grünwald V, Hutson TE, Kopyltsov E, Méndez-Vidal MJ, Kozlov V, Alyasova A, Hong SH, Kapoor A, Alonso Gordoa T, Merchan JR, Winquist E, Maroto P, Goh JC, Kim M, Gurney H, Patel V, Peer A, Procopio G, Takagi T, Melichar B, Rolland F, De Giorgi U, Wong S, Bedke J, Schmidinger M, Dutcus CE, Smith AD, Dutta L, Mody K, Perini RF, Xing D and Choueiri TK; CLEAR Trial Investigators. Lenvatinib plus pembrolizumab or everolimus for advanced renal cell carcinoma. N Engl J Med 2021; 384: 1289-1300.
[37] Motzer RJ, Tannir NM, McDermott DF, Arén Frontera O, Melichar B, Choueiri TK, Plimack ER, Barthélémy P, Porta C, George S, Powles T, Donskov F, Neiman V, Kollmannsberger CK, Salman P, Gurney H, Hawkins R, Ravaud A, Grimm MO, Bracarda S, Barrios CH, Tomita Y, Castellano D, Rini BI, Chen AC, Mekan S, McHenry MB, Wind-Rotolo M, Doan J, Sharma P, Hammers HJ and Escudier B; CheckMate 214 Investigators. Nivolumab plus ipilimumab versus sunitinib in advanced renal-cell carcinoma. N Engl J Med 2018; 378: 1277-1290.
[38] Au L, Hatipoglu E, Robert de Massy M, Litchfield K, Beattie G, Rowan A, Schnidrig D, Thompson R, Byrne F, Horswell S, Fotiadis N, Hazell S, Nicol D, Shepherd STC, Fendler A, Mason R, Del Rosario L, Edmonds K, Lingard K, Sarker S, Mangwende M, Carlyle E, Attig J, Joshi K, Uddin I, Becker PD, Sunderland MW, Akarca A, Puccio I, Yang WW, Lund T, Dhillon K, Vasquez MD, Ghorani E, Xu H, Spencer C, López JI, Green A, Mahadeva U, Borg E, Mitchison M, Moore DA, Proctor I, Falzon M, Pickering L, Furness AJS, Reading JL, Salgado R, Marafioti T, Jamal-Hanjani M; PEACE Consortium, Kassiotis G, Chain B, Larkin J, Swanton C,

Quezada SA and Turajlic S; TRACERx Renal Consortium. Determinants of anti-PD-1 response and resistance in clear cell renal cell carcinoma. Cancer Cell 2021; 39: 1497-1518, e11.

[39] Labriola MK, Zhu J, Gupta RT, McCall S, Jackson J, Kong EF, White JR, Cerqueira G, Gerding K, Simmons JK, George D and Zhang T. Characterization of tumor mutation burden, PD-L1 and DNA repair genes to assess relationship to immune checkpoint inhibitors response in metastatic renal cell carcinoma. J Immunother Cancer 2020; 8: e000319.

[40] Braun DA, Hou Y, Bakouny Z, Ficial M, Sant' Angelo M, Forman J, Ross-Macdonald P, Berger AC, Jegede OA, Elagina L, Steinharter J, Sun M, Wind-Rotolo M, Pignon JC, Cherniack AD, Lichtenstein L, Neuberg D, Catalano P, Freeman GJ, Sharpe AH, McDermott DF, Van Allen EM, Signoretti S, Wu CJ, Shukla SA and Choueiri TK. Interplay of somatic alterations and immune infiltration modulates response to PD-1 blockade in advanced clear cell renal cell carcinoma. Nat Med 2020; 26: 909-918.

[41] Benhamouda N, Sam I, Epaillard N, Gey A, Phan L, Pham HP, Gruel N, Saldmann A, Pineau J, Hasan M, Quiniou V, Nevoret C, Verkarre V, Libri V, Mella S, Granier C, Broudin C, Ravel P, De Guillebon E, Mauge L, Helley D, Jabla B, Chaput N, Albiges L, Katsahian S, Adam J, Mejean A, Adotevi O, Vano YA, Oudard S and Tartour E. Plasma CD27, a surrogate of the intratumoral CD27-CD70 interaction, correlates with immunotherapy resistance in renal cell carcinoma. Clin Cancer Res 2022; 28: 4983-4994.

[42] Hoxhaj G and Manning BD. The PI3K-AKT network at the interface of oncogenic signalling and cancer metabolism. Nat Rev Cancer 2020; 20: 74-88.

[43] Faubert B, Solmonson A and DeBerardinis RJ. Metabolic reprogramming and cancer progression. Science 2020; 368: eaaw5473.

[44] Fu X, Tang N, Xie WQ, Mao L and Qiu YD. MUC1 promotes glycolysis through inhibiting BRCA1 expression in pancreatic cancer. Chin J Nat Med 2020; 18: 178-185.

[45] Lee P, Malik D, Perkons N, Huangyang P, Khare S, Rhoades S, Gong YY, Burrows M, Finan JM, Nissim I, Gade TPF, Weljie AM and Simon MC. Targeting glutamine metabolism slows soft tissue sarcoma growth. Nat Commun 2020; 11: 498.

[46] Wu L, Wang W, Dai M, Li H, Chen C and Wang D. PPARalpha ligand, AVE8134, and cyclooxygenase inhibitor therapy synergistically suppress lung cancer growth and metastasis. BMC Cancer 2019; 19: 1166.

[47] Lucarelli G, Rutigliano M, Sallustio F, Ribatti D, Giglio A, Lepore Signorile M, Grossi V, Sanese P, Napoli A, Maiorano E, Bianchi C, Perego RA, Ferro M, Ranieri E, Serino G, Bell LN, Ditonno P, Simone C and Battaglia M. Integrated multiomics characterization reveals a distinctive metabolic signature and the role of NDUFA4L2 in promoting angiogenesis, chemoresistance, and mitochondrial dysfunction in clear cell renal cell carcinoma. Aging (Albany NY) 2018; 10: 3957-3985.

[48] Vuong L, Kotecha RR, Voss MH and Hakimi AA. Tumor microenvironment dynamics in clear-cell renal cell carcinoma. Cancer Discov 2019; 9: 1349-1357.

[49] Borcherding N, Vishwakarma A, Voigt AP, Bellizzi A, Kaplan J, Nepple K, Salem AK, Jenkins RW, Zakharia Y and Zhang W. Mapping the immune environment in clear cell renal carcinoma by single-cell genomics. Commun Biol 2021; 4: 122.

[50] Mu X, Shi W, Xu Y, Xu C, Zhao T, Geng B, Yang J, Pan J, Hu S, Zhang C, Zhang J, Wang C, Shen J, Che Y, Liu Z, Lv Y, Wen H and You Q. Tumor-derived lactate induces M2 macrophage polarization via the activation of the ERK/STAT3 signaling pathway in breast cancer. Cell Cycle 2018; 17: 428-438.

[51] Angelin A, Gil-de-Gómez L, Dahiya S, Jiao J, Guo L, Levine MH, Wang Z, Quinn WJ 3rd, Kopinski PK, Wang L, Akimova T, Liu Y, Bhatti TR, Han R, Laskin BL, Baur JA, Blair IA, Wallace DC, Hancock WW and Beier UH. Foxp3 reprograms T cell metabolism to function in low-glucose, high-lactate environments. Cell Metab 2017; 25: 1282-1293, e7.

[52] Zappasodi R, Serganova I, Cohen IJ, Maeda M, Shindo M, Senbabaoglu Y, Watson MJ, Leftin A, Maniyar R, Verma S, Lubin M, Ko M, Mane MM, Zhong H, Liu C, Ghosh A, Abu-Akeel M, Ackerstaff E, Koutcher JA, Ho PC, Delgoffe GM, Blasberg R, Wolchok JD and Merghoub T. CTLA-4 blockade drives loss of T(reg) stability in glycolysis-low tumours. Nature 2021; 591: 652-658.

[53] Feng G, Shi H, Li J, Yang Z, Fang R, Ye L, Zhang W and Zhang X. MiR-30e suppresses proliferation of hepatoma cells via targeting prolyl 4-hydroxylase subunit alpha-1 (P4HA1) mRNA. Biochem Biophys Res Commun 2016; 472: 516-522.

[54] Atkinson A, Renziehausen A, Wang H, Lo Nigro C, Lattanzio L, Merlano M, Rao B, Weir L, Evans A, Matin R, Harwood C, Szlosarek P, Pickering JG, Fleming C, Sim VR, Li S, Vasta JT, Raines RT, Boniol M, Thompson A, Proby C, Crook T and Syed N. Collagen prolyl hydroxylases are bifunctional growth regulators in melanoma. J Invest Dermatol 2019; 139: 1118-1126.

[55] Winslow S, Lindquist KE, Edsjo A and Larsson C. The expression pattern of matrix-producing tumor stroma is of prognostic importance in breast cancer. BMC Cancer 2016; 16: 841.
[56] Song H, Liu L, Song Z, Ren Y, Li C and Huo J. P4HA3 is Epigenetically activated by slug in gastric cancer and its deregulation is associated with enhanced metastasis and poor survival. Technol Cancer Res Treat 2018; 17: 1533033818796485.
[57] Guan Y, Chen X, Wu M, Zhu W, Arslan A, Takeda S, Nguyen MH, Majeti R, Thomas D, Zheng M and Peltz G. The phosphatidylethanolamine biosynthesis pathway provides a new target for cancer chemotherapy. J Hepatol 2020; 72: 746-760.
[58] Bi J, Ichu TA, Zanca C, Yang H, Zhang W, Gu Y, Chowdhry S, Reed A, Ikegami S, Turner KM, Zhang W, Villa GR, Wu S, Quehenberger O, Yong WH, Kornblum HI, Rich JN, Cloughesy TF, Cavenee WK, Furnari FB, Cravatt BF and Mischel PS. Oncogene amplification in growth factor signaling pathways renders cancers dependent on membrane lipid remodeling. Cell Metab 2019; 30: 525-538, e8.
[59] Kamdar S, Isserlin R, Van der Kwast T, Zlotta AR, Bader GD, Fleshner NE and Bapat B. Exploring targets of TET2-mediated methylation reprogramming as potential discriminators of prostate cancer progression. Clin Epigenetics 2019; 11: 54.
[60] Kono N, Inoue T, Yoshida Y, Sato H, Matsusue T, Itabe H, Niki E, Aoki J and Arai H. Protection against oxidative stress-induced hepatic injury by intracellular type II platelet-activating factor acetylhydrolase by metabolism of oxidized phospholipids in vivo. J Biol Chem 2008; 283: 1628-1636.
[61] Ge J, Yu Y, Xin F, Yang ZJ, Zhao HM, Wang X, Tong ZS and Cao XC. Downregulation of delta-aminolevulinate dehydratase is associated with poor prognosis in patients with breast cancer. Cancer Sci 2017; 108: 604-611.

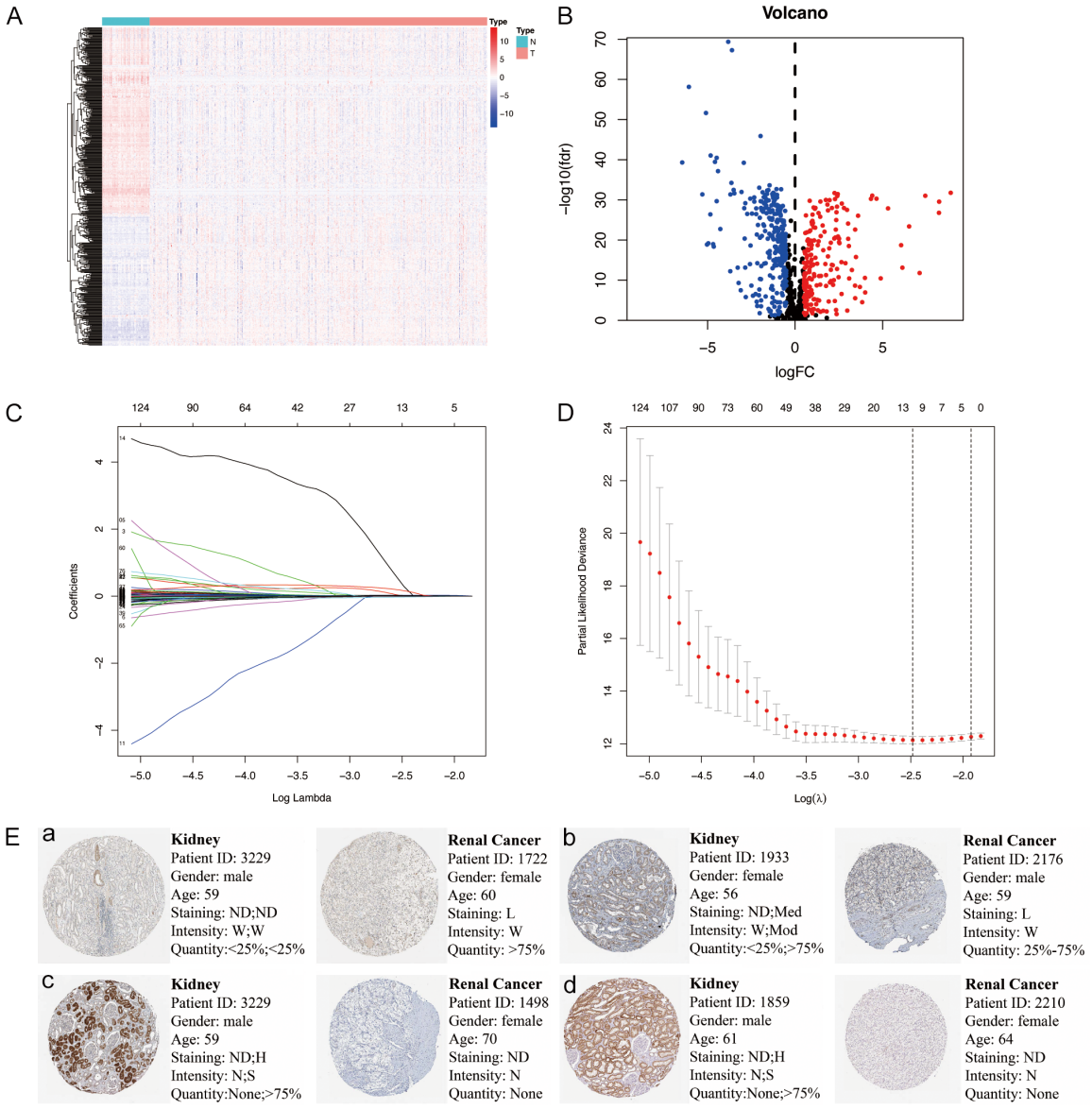

Figure S1. Identification of differentially expressed MGs and further analysis of the prognostic differentially expressed MGs in the training cohort. A. Heat map of MGs; the blue to red spectrum indicates low to high gene expression. B. Volcano plot of MGs; the blue dots represent downregulated MGs, the red dots represent upregulated MGs and the black dots represent MGs that were not significantly differentially expressed. C, D. Prognostic differentially expressed MGs selected through Lasso regression. E. Validation of risk genes at the protein level by The Human Protein Atlas database (IHC). a. Expression of P4HA3 in normal kidney tissue and renal cancer tissue (40×). b. Expression of PAFAH2 in normal kidney tissue and renal cancer tissue (40×). c. Expression of ALAD in normal kidney tissue and renal cancer tissue (40×). d. Expression of ETNK2 in normal kidney tissue and renal cancer tissue (40×). In normal tissues, there are two types of IHC. The former refers to the staining state of cells in glomeruli, the latter refers to the staining state of cells in tubules. Abbreviations: L, Low; Med, Medium; H, High; ND, not detected; W, Weak; Mod, Moderate; S, Strong; N, None.

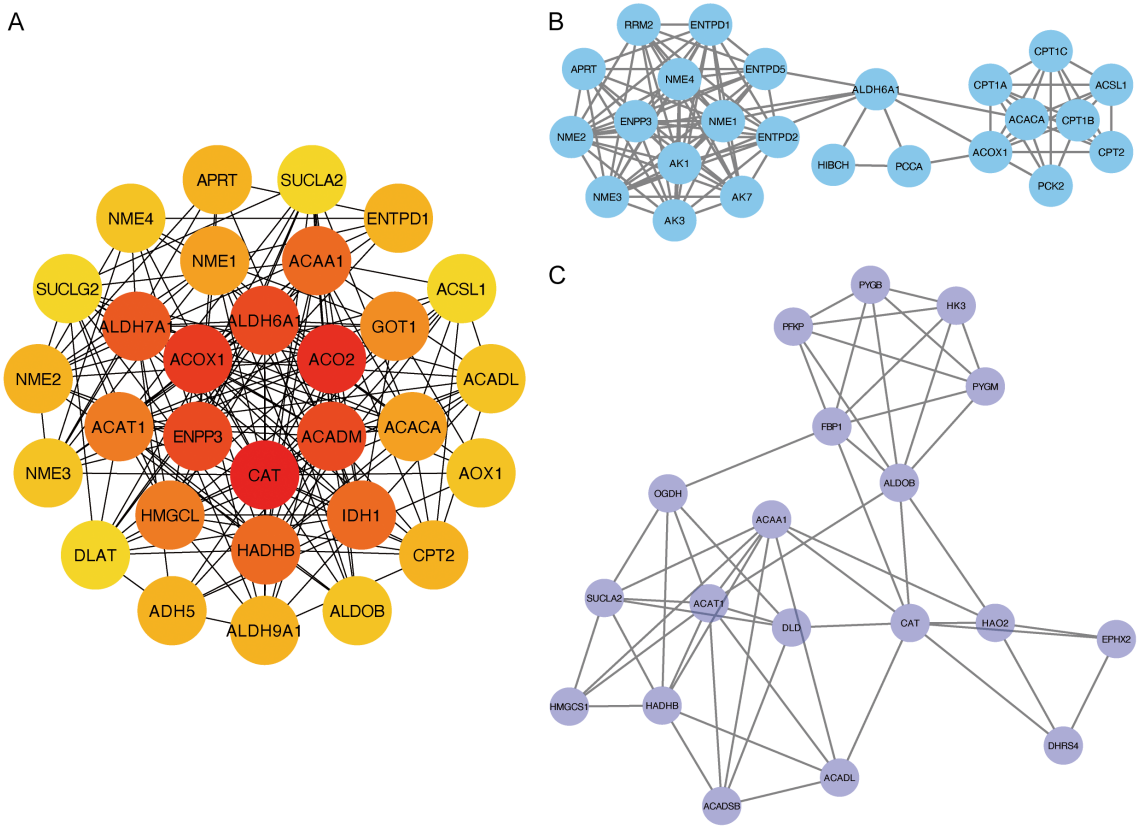

Figure S2. The protein-protein interaction (PPI) network of top 30 hub genes, as well as top 2 modules were constructed. A. The PPI network of the intersects genes. B, C. Top 2 hub modules were identified by MCODE.

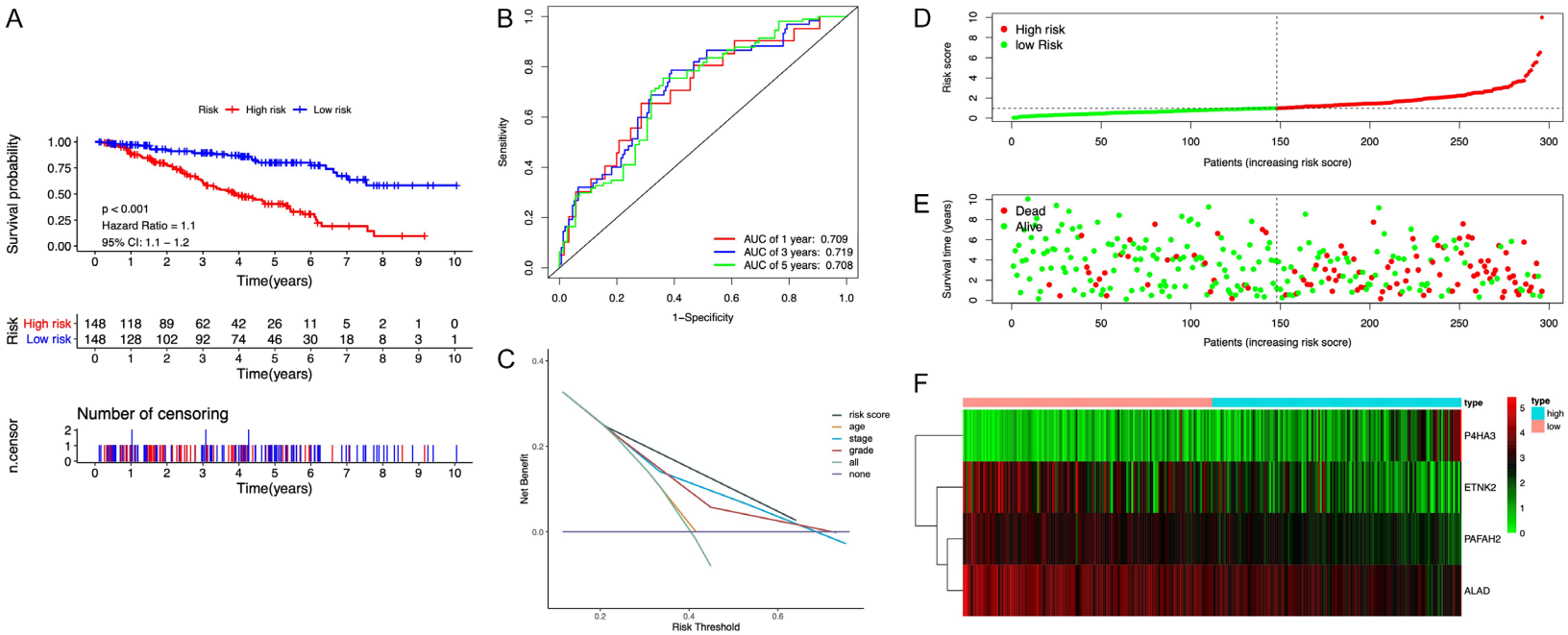

Figure S3. Prognostic analysis of the prognostic model in training cohort. A. Kaplan-Meier curve analysis of the high-risk and low-risk groups. B. Time-dependent ROC curve analysis of the prognostic model. C. DCA analysis of different variables in training cohort. D. Risk score distribution of patients in the prognostic model. E. Survival status scatter plots for patients in the prognostic model. F. Expression patterns of risk genes in the prognostic model.

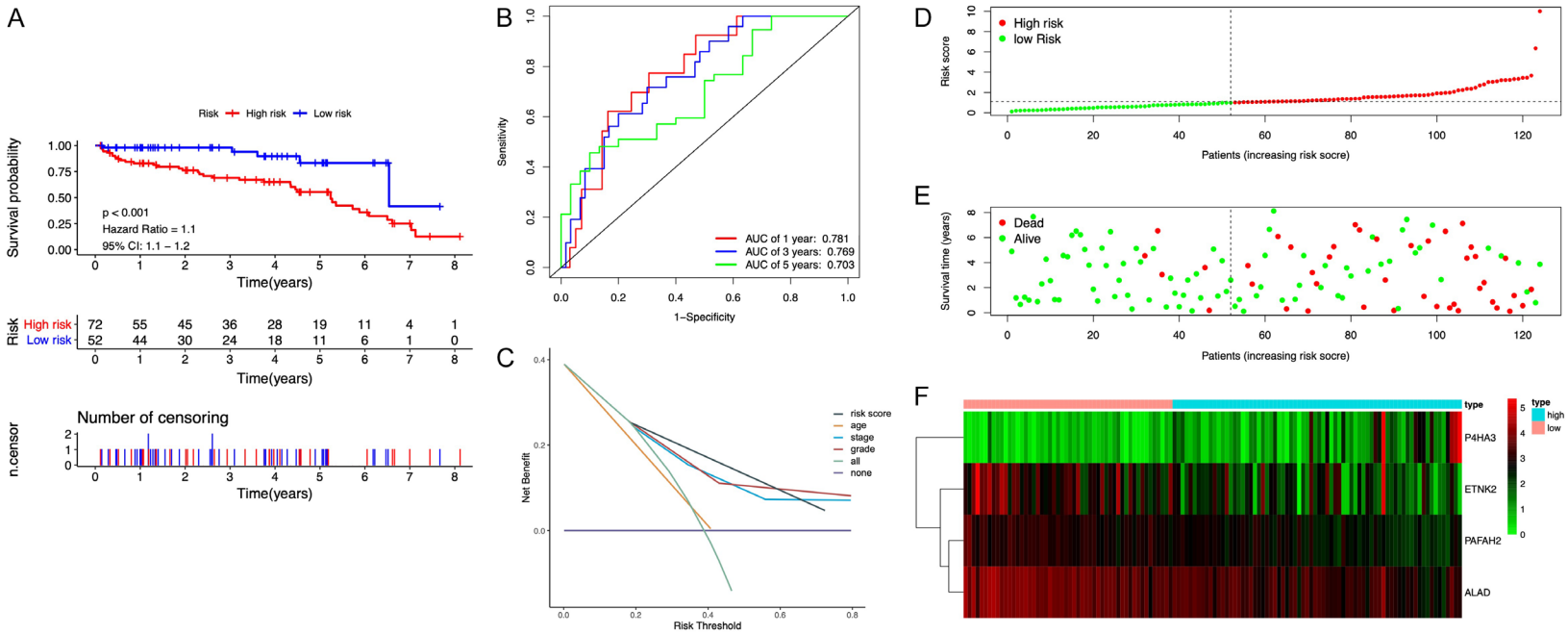

Figure S4. Prognostic analysis of the prognostic model in testing cohort. A. Kaplan-Meier curve analysis of the high-risk and low-risk groups. B. Time-dependent ROC curve analysis of the prognostic model. C. DCA analysis of different variables in testing cohort. D. Risk score distribution of patients in the prognostic model. E. Survival status scatter plots for patients in the prognostic model. F. Expression patterns of risk genes in the prognostic model.

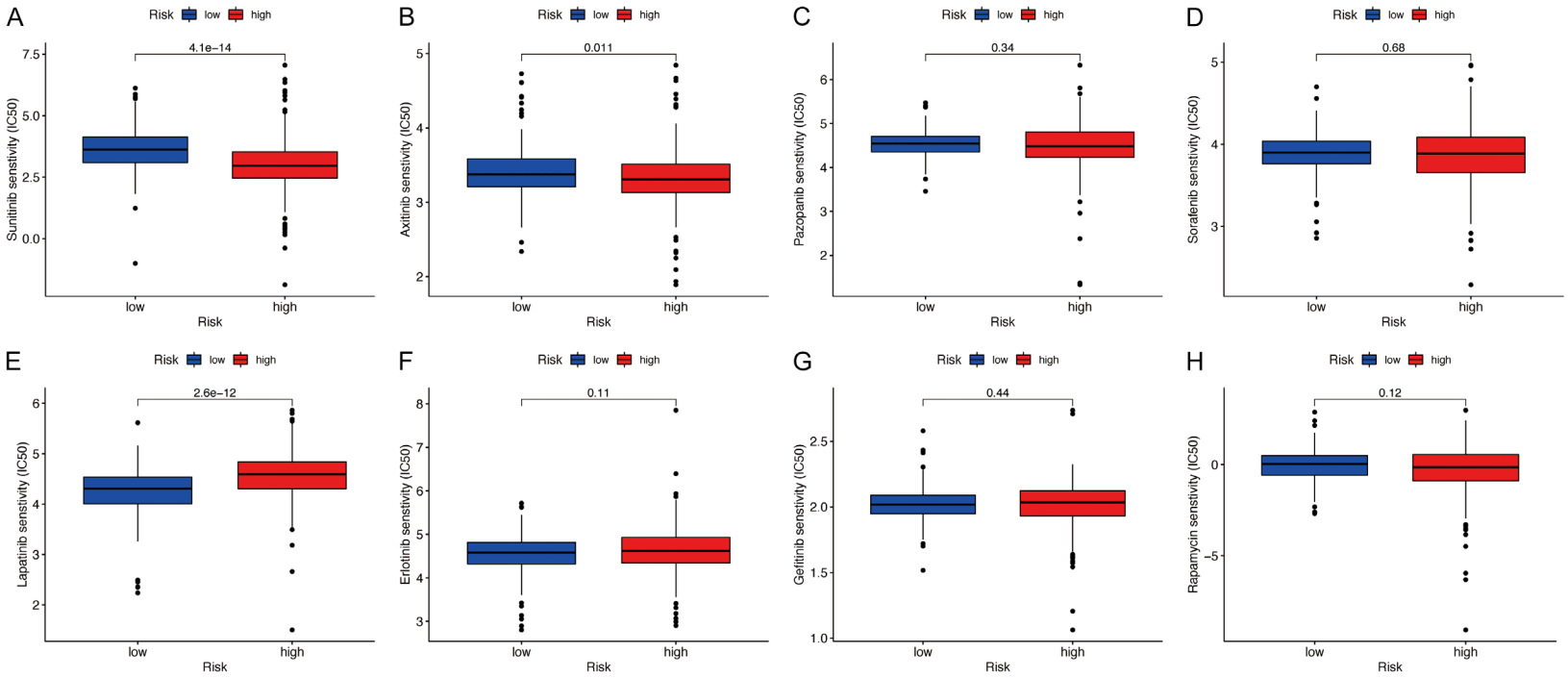

Figure S5. The drug sensitivity of eight common targeted compounds. A. IC50 of sunitinib in the high-risk and low-risk groups. B. IC50 of axitinib in the high-risk and low-risk groups. C. IC50 of pazopanib in the high-risk and low-risk groups. D. IC50 of sorafenib in the high-risk and low-risk groups. E. IC50 of lapatinib in the high-risk and low-risk groups. F. IC50 of eriotinib in the high-risk and low-risk groups. G. IC50 of gefitinib in the high-risk and low-risk groups. H. IC50 of rapamycin in the high-risk and low-risk groups.